MOBIDYCS

Integrating bioturbation and biodeposition processes in hydrodynamic and transport models for contaminated sediments

Progress report

MARETEC - IST

February 2004

INDEX

Introduction

This report was developed in the framework of the MOBIDYCS project, regarding MARETEC tasks progress during the past year of 2003.

Overview

The main advances in the framework of this project during 2003 were:

- ADV measurements performed in the annular channel, used to compare and calibrate modelling results;
- model applications at the annular channel scale using two different models: MOHID, develop at Instituto Superior Técnico, and FLUENT, a commercial flow modelling package, and respective comparison with measured results;
- Improvements were made in MOHID modelling system regarding general restructuring and more specifically, the improvement of the cyclic boundary condition used in the annular channel modelling applications.

The option of using a second, and more specific model like FLUENT, was to use the experience that this kind of models have in small scale applications, such as annular flumes, in order to calibrate MOHID hydrodynamics when applying it to the channel.

This work will ultimately result in better hydrodynamic interpretation, enabling the comparison with other laboratory experimental results that will be used to support the sediment and contaminant transport and biogeochemical model. Afterwards, the model will be applied to estuarine and coastal systems, representing then an important step to better describe and understand the complex occurring processes.

Methodology

Modelling tools I: Mohid

MOHID is a modular finite volumes water modelling system written in ANSI FORTRAN 95 using an object oriented programming philosophy, integrating about a dozen programs written in FORTRAN 95 and supported by graphical user interfaces both in FORTRAN (using OpenGL libraries) and Microsoft Visual Basic .NET. It is an integrated modelling tool able to simulate processes in a water column and in the sediments and the coupling between these two domains and the atmosphere.

The water column model, MOHID Water, is composed by a free surface three-dimensional baroclinic hydrodynamic module, a turbulence module (including GOTM), an eulerian transport module, a lagrangian transport module, an oil dispersion model and a three zero-dimensional biogeochemical modules. The sediments model is composed by a saturated one-dimensional consolidation, an eulerian transport model and by a zero-dimensional sediment quality/biogeochemical model. Atmospheric processes can be included by imposing atmospheric observed data or atmospheric model results.

Model applications

The model has been applied to several coastal and estuarine areas and it has showed its ability to simulate complex features of the flows. Several different coastal areas have been modelled with MOHID in the framework of research and consulting projects. Along the Portuguese coast, different environments have been studied, including the main estuaries (Minho, Lima, Douro, Mondego, Tejo, Sado, Mira, Arade and Guadiana) and coastal lagoons (Ria de Aveiro and Ria Formosa), INAG [2001]; Martins et al. (2000). The model has been also implemented in most Galician Rías: Ría de Vigo by Taboada *et al*., (1998), Montero, (1999) and Montero *et al*. [1999], Ría de Pontevedra by Taboada *et al.* [2000] and Villarreal *et al.* [2000] and in other Rías by Pérez Villar *et al* [1999].

Some North European estuaries have also been modelled - Western Scheldt, The Netherlands, Gironde, France by Cancino and Neves, [1999] and Carlingford, Ireland, by Leitão, [1997] - as well as some estuaries in Brasil (Santos SP and Fortaleza).

Regarding to open sea, MOHID has been applied to the North-East Atlantic region where some processes including the Portuguese coastal current, Coelho (2002), the slope current along the European Atlantic shelf break, Neves *et al*. (1998) and the generation of internal tides, Neves *et al*. (1998) have been studied and also to the Mediterranean Sea to simulate the seasonal cycle, Taboada, (1999) or the circulation in the Alboran Sea, Santos, (1995).

More recently MOHID has been applied to the several Portuguese fresh water reservoirs Monte Novo, Roxo and Alqueva, (Braunschweig, 2001), in order to study the flow and water quality.

Model structure

MOHID modular structure enables that each module can correspond to a different compartment (water column, sediments, and atmosphere) or to a specific process or set of processes, that is, each module is responsible to manage a certain kind of information. For example module “WaterProperties” is responsible for computing the properties evolution in the water column, corresponding in this case to the water column domain. To do so, this module uses other modules, responsible for specific processes like module “AdvectionDiffusion” which computes properties transport, or module “WaterQuality” which computes properties biogeochemical reactions, and so on.

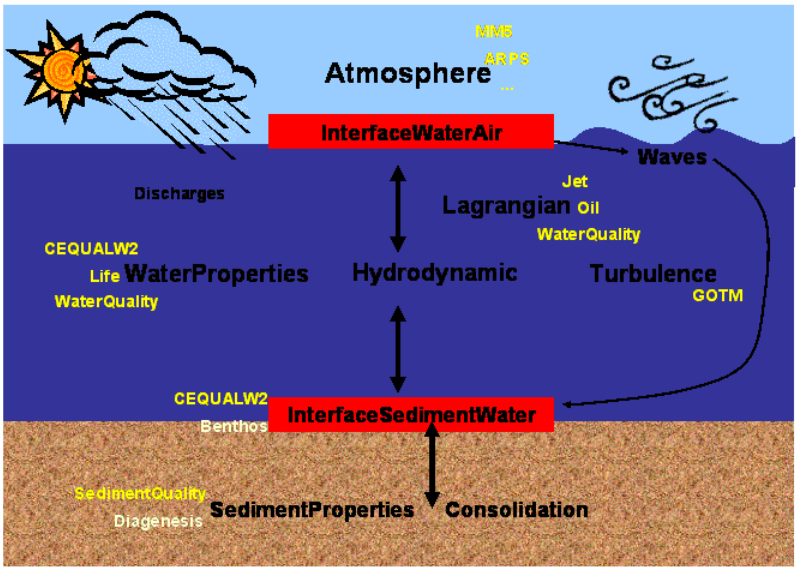

Figure 1 - Mohid modular structure (main modules)

In terms of global organization, MOHID can be divided in the water column (module "WaterProperties" and module "Hydrodynamic"), in the sediment compartment (module "SedimentProperties") and the atmosphere (module "Atmosphere"). Each compartment is separated by an interface, which controls the information and communications between two domains, namely the "InterfaceWaterAir" module and the "InterfaceSedimentWater" module. MOHID does not explicitly compute the atmosphere processes. Module "Atmosphere" works as a database module, in which this processes are given to the model as inputs, with origin in atmospheric observed data or in atmospheric model results.

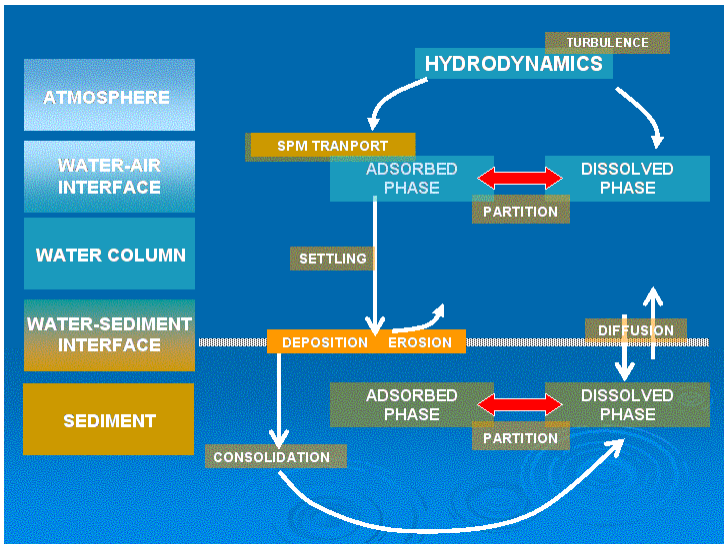

Figure 2 – Water-sediment interface processes in Mohid

The water column

The water column entity is, as said, module "WaterProperties". This module uses module "Hydrodynamic" to compute water fluxes that are then used to compute properties transport (see Annexe 1 for technical description). MOHID is prepared to simulate properties such temperature, salinity, cohesive sediments, phytoplankton, nutrients, contaminants, etc. These properties can be considered as being dissolved in the water, therefore following the currents, or as being particulate or adsorbed on to particulate matter, thus being subjected to one more transport variable: the settling velocity. This causes particulate properties to deposit in the bottom and thus become a part of the sediments.

The ability to simulate different properties in both dissolved and particulate states is an important feature included in the model. But probably even more important, is the possibility of computing the distribution of a property between the solid and the dissolved phase, using a partition coefficient formulation. This is a very common modelling approach to simulate transport and fate of contaminants. In these cases the roll of particulate matter is very important, namely the through cohesive sediment transport, due to the important percentage of, not only, contaminants adsorbed on to its surface, but also due to the fraction of organic matter that is part of this kind of sediments and that influences the nutrient cycling in marine systems.

The water-sediment interface

Module “InterfaceSedimentWater”, the entity for water-sediment interface, controls the cohesive sediment fluxes between the water-column and the sediments, namely through computing erosion and through enabling deposition, both processes being determined by the flow intensity near the bottom, in the form of shear stress. The water-sediment interface is a zone with transient characteristics, and it can be seen as a thin high porous layer constituted of water and sediments. The processes that take place here depend on the processes taking place above, in the water column, and below in the “quiet” sediment. For example, once deposited in the bottom, particulate matter can either stay there or be resuspended back to the water column. If the tendency is to remain deposited, that is, if the deposition flux is higher than the erosion flux, then it becomes part of the sediment. This source to the sediment compartment is computed as a consolidation rate applied to the deposited particulate matter. This is true not only as a sediment source, as well as a source of adsorbed properties to the sediment compartment. On the other hand, if the erosion flux is very high, and the particulate matter deposited in the water-sediment interface is fully eroded, the upper sediment layers can be eroded, depending, in this case, on their characteristics.

Dissolved properties fluxes depend on water flow across the water-sediment interface and on concentration gradients between the water column’s lower layer concentration and the concentration on the interstitial water of the sediment’s upper layer. Therefore one can divide this boundary fluxes on an advective flux and a diffusive flux. For the latter, the rate at which the gradient tends to be eliminated depends on the water column flow, i.e. on the bottom shear stress. Therefore, it is considered a bottom shear stress dependent mass transfer coefficient.

Benthic filter-feeders, macro-algae and other benthic organisms interacting with the water column and the sediment are also managed (or to be managed) by the module “InterfaceSedimentWater”.

The sediment compartment

The model structure used for simulating sediments is very similar with the one used to simulate the water column. The most important modules are, in this case, module "Consolidation", module "AdvectionDiffusion" and module "SedimentQuality.

The MOHID's sediment compartment is seen as a media composed of sediment, water and in some cases air. Properties, in resemblance to the "WaterProperties" module, can either be dissolved in the interstitial water or adsorbed onto the sediment. They also can be specific of the sediment or they can interact with the water column. Module "Consolidation" is responsible for computing the water flow within the sediment layers and is a simple consolidation model that considers a consolidation rate, at which the sediment layers compact. This is achieved with an interstice volume decay rate, reducing water content in the sediments and leading to an upward movement of the interstitial water till it reaches the water column. These water fluxes can become important, as they are responsible for advective transport of dissolved properties to the water column. Saturated conditions are considered, resulting in a simple formulation to compute the water velocity. This module receives as initial inputs the water content, the consolidation rate parameters and in run-time it receives a sediment flux from the water column, through module "InterfaceSedimentWater", due to particulate matter settling.

Module "AdvectionDiffusion" solves the mass transport equations using the water fluxes computed by the interface module "SedimentHydrodynamic".

Module "SedimentQuality" is a biogeochemical model, based on RZWQM/OMNI, for carbon and nitrogen cycling in soils (unsaturated porous media), presently being prepared to be adapted to estuarine and marine saturated sediments, as it includes already bacterial (autotrophic, heterotrophic and anaerobic) growth/organic matter mineralization with oxygen balance.

Modelling tools II: FLUENT

FLUENT is a hydrodynamic modelling commercial package based in a finite volume approach, similarly to MOHID. As it is usually the case with commercial products, FLUENT provides a large variety of models for solving the hydrodynamic flows. It is up to the user to choose the best-suited model for his case.

The applicable model for solving free-surface flow with FLUENT is the Volume of Fluid (VOF) model. The VOF formulation relies on the fact that two or more fluids (or phases) are not interpenetrating. It is a general model that allows considering multiple fluids (or phases) but for simplicity we will describe it for our case. Let α be the water volume fraction.

According to the model, three conditions are possible:

- = 0, the cell is empty of water;
- = 1, the cell is full of water;
- $0 < \alpha < 1$, the cell contains the interface between air and water.

The variable and properties in any cell are either purely representative of one of the phases, or representative of a mixture of the phases.

Based on the local value of the appropriate properties and variables will be assigned to each control volume within the domain.

In the case the cell is at the interface the fields for all variables and properties are shared by the phases and represent volume-averaged values. For a given property ϕ, with ϕ_w and ϕ_a water and air respective values, the cell average is:

$$\phi = \alpha\phi_w + (1-\alpha)\phi_a$$

The tracking of the interface between phases is accomplished by the solution of a continuity equation for the volume fraction of one of the phases:

$$\frac{\partial \alpha}{\partial t} + \vec{v} \cdot \vec{\nabla}\alpha = 0$$

A single momentum equation is solved throughout the domain, and the resulting velocity field is shared among the phases. The momentum is dependent on the volume fractions of all phases through the properties ρ and μ.

One limitation of the shared-fields approximation is that in cases where large velocity differences exist between the phases, the accuracy of the velocities computed near the interface can be adversely affected. It is not our case because we expect continuity between velocities (omitting surface tension, this affirmation is true).

Turbulence Modelling – the k-ε RNG model

Main concern regards the turbulence model, because it is turbulence that originates the secondary flow. The k-ε model is a widely used turbulence model, mostly for industrial applications. It is a two model equations with potential as it has been seen in the years. Although its validity is permanently contested, it is still one of the few that can be used for very complex applications. "The k-ε is arguably the simplest complete turbulence model, and hence it has the broadest range of applicability" (Pope, 2000).

While waiting for computers that work with terabytes of RAM so they are able to sustain LES calculations for intricate geometries, it is useful to see how far the model goes.

It is, at least, good for depicting the main features of simple flows as will be shown in this study and gives a quick answer to a practical problem. Comparison with (Schweim, 2000) will show how this approach is desirable compared to LES.

In this study a widespread variant of k-ε is used: the k-ε RNG. The standard k-ε model assumes (Pope, 2000):

- the turbulent viscosity hypothesis (deviatoric Reynold stress is proportional to mean rate of strain):

$$-\rho\left\langle u_i v_j \right\rangle + \frac{2}{3}\rho k \delta_{ij} = \rho \nu_T \left(\frac{\partial \left\langle U_i \right\rangle}{\partial x_j} + \frac{\partial \left\langle U_i \right\rangle}{\partial x_j} \right)$$

- ν_T, the turbulent viscosity, is supposed to depend only on k and ε which leads to:

$$\nu_T = C_\mu \frac{k^2}{\varepsilon}$$

where C_μ is a constant.

Based on this, the model is set with one transport equation for k and another for ε (the former is the exact equation while the latest is empirical), which along with the preceding equation closes the system.

The RNG-based k-ε turbulence model is derived from the instantaneous Navier-Stokes equations, using a mathematical technique called "renormalization group" (RNG) methods. The analytical derivation results in a model with constants different from those in the standard k-ε model, and additional terms and functions in the transport equations for k and ε.

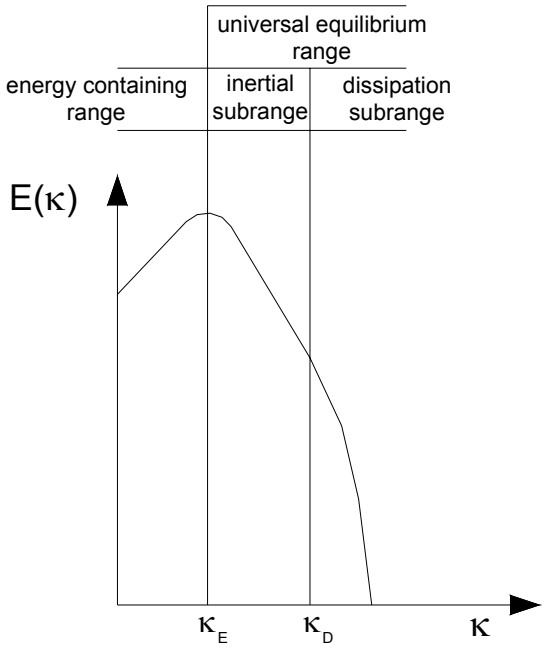

Figure 3 –Scales of turbulent motion: energy spectra against wave-number (log-log plot)

ReNormalisation Group (RNG) methods provide a general set of rules which allow physical problems to be expressed in terms of equations governing the large-scale, long-time behaviour of the system.

According to the Kolmogorov hypothesis, in any turbulent flow a sufficiently large Reynolds number, the high wave-number portion of the velocity spectra adopts universal forms. The high wave-number portion of velocity spectra correspond to small motion scales. In these conditions the flow can be characterized by three ranges of spatial scales **(**Croft, 1998**)**:

- **Energy containing range ($\kappa<\kappa_E$)**: the energy spectrum is strongly anisotropic as well as being non universal for wave numbers $\kappa = O(\pi/L)$. In this range the

integral scale is affected by booth the geometry of the flow and the physicochemical processes taking place.

- **Inertial sub-range ($\kappa_E < \kappa < \kappa_D$)**: at smaller scales, the inertial range of small scale eddies, the velocity fluctuation spectrum, $E(\kappa)$, is approximately given by Kolmogorov law:

$$E(\kappa) = C_k \varepsilon^{2/3} k^{-5/3}$$

- **Dissipation range ($\kappa > \kappa_D$)**: for highest wave-numbers ($\kappa = O(\kappa_D)$), the eddies have very low energy due to viscous dissipation. In this range the energy spectrum decreases exponentially with κ

The two last ranges form the *universal equilibrium range* because it is valid for any turbulent flow. A typical energy spectrum is represented in **Figure 3**.
Once the inertial range of eddies have been expressed in a quantitative accurate manner, the RNG methods can be applied to obtain coarse-grained equations for the turbulence related variables.

The range of scales of the effective excitation in turbulence lie between the low, energy containing wave-number κ_E and the high wave-number viscous cutoff, κ_D. The RNG method removes a narrow band of modes near κ_D by expressing them in terms of lower modes. Having removed this band of modes, the equations of motion for the remaining modes is a modified system of Navier-Stokes equations (that does not take into account smallest scales of turbulent motion). In practice, the RNG method produces a form of the Navier-Stokes equation which allows the computation on coarser grids.

Wall Boundary Condition – Tow Boundary Layer

To model the flow in the vicinity of the wall a low Reynolds solver is used for the laminar sub-layer. The constants of the k-e model (C_μ, $C_{\varepsilon 1}$, $C_{\varepsilon 2}$) are algebraic function of the distance to the wall **(**Viollet et al, 1998**)**.

In this approach the whole domain is subdivided into a viscosity-affected and fully-turbulent region. The demarcation of the two regions is determined by a wall-distance based, turbulent Reynolds number Re_y, defined as [3]:

$$\mathrm{Re}_y = \frac{y\sqrt{k}}{\nu}$$

where y is the normal distance from the wall at the cell centers.

This model requires that the mesh is sufficiently refined in the laminar sub-layer to work ($y^+ \cong 1$). Fluent provides a more flexible model called "Enhanced Wall Treatment" which uses the low Reynolds solver when applicable (i.e. the grid is fine enough) and wall functions elsewhere, which do not require such a refined grid ($y^+ \cong$ 100 to 300).

Convergence Criteria

Convergence of the numerical system is given by the residuals. After discretization, the conservation equation for a variable ϕ in a generic cell P can be written in the form:

$$a_P\phi_P = \sum_l a_l\phi_l + b$$

where a_P is the center coefficient, a_l are the coefficients of neighboring cells, and b is the constant part of the source terms (the remaining is included in the a_i).

Residuals are defined as a sum over all cells of the domain:

$$R^\phi = \sum_{cells}\left|\sum_l a_l\phi_l + b - a_P\phi_P\right|$$

The residuals are usually scaled:

$$R^\phi = \frac{\sum_{cells}\left|\sum_l a_l\phi_l + b - a_P\phi_P\right|}{\sum_{cells} a_P\phi_P}$$

Experience recommends considering 10^{-3} to 10^{-4} for industrial flows, but 10^{-6} at research level.

Laboratory data measurements

Laboratory data measurements were performed in the annular channel using an ADV currentmeter (Sontek® Micro-ADV).

Scenarios

Four scenarios were set up for performing measurements, namely through applying four different rotation velocities to the channel plate, representing four stabilized flow fields.

Each velocity scenario was defined by measuring approximate velocities of 5, 10, 20 and 40 cm/s at 10 cm above the bottom of the channel, after 5 minutes stabilization. Velocities were measured in the centre of the flume (width = 10 cm) along the vertical axis from the bottom of the channel till 15 cm above. The profile points were chosen in order to present a denser distribution near the bottom, where gradients are higher, so that a better discretization was observed.

Results

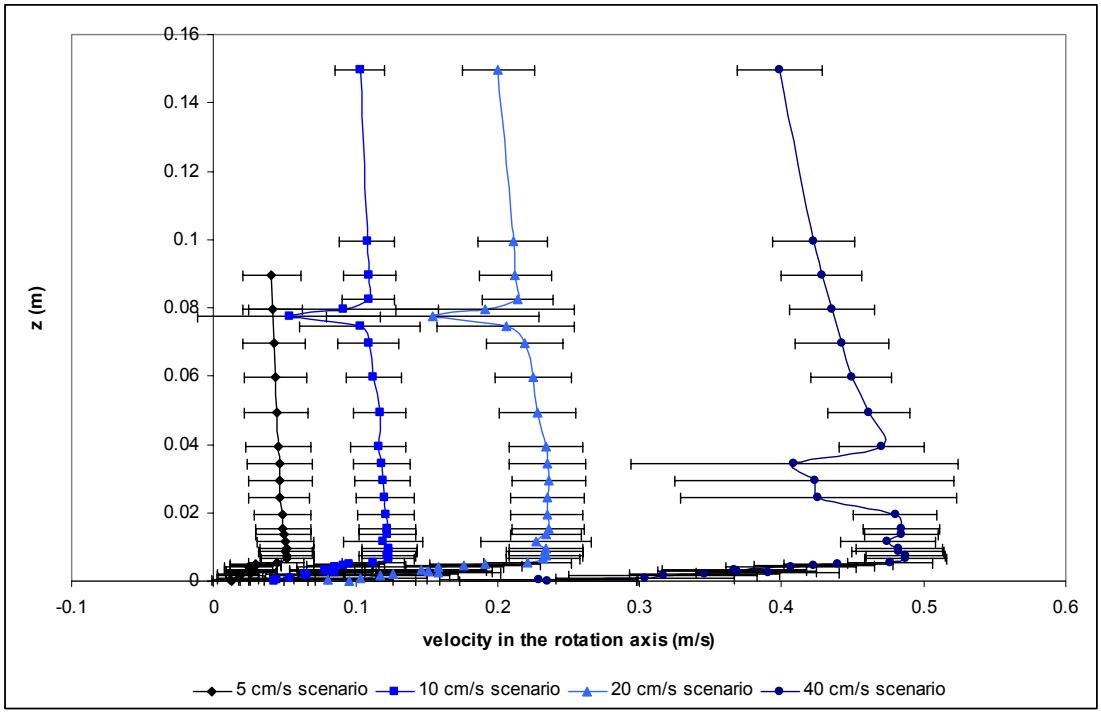

Figure 4 – Mean velocities along rotation axis for the four scenarios (error bars represent standard deviation)

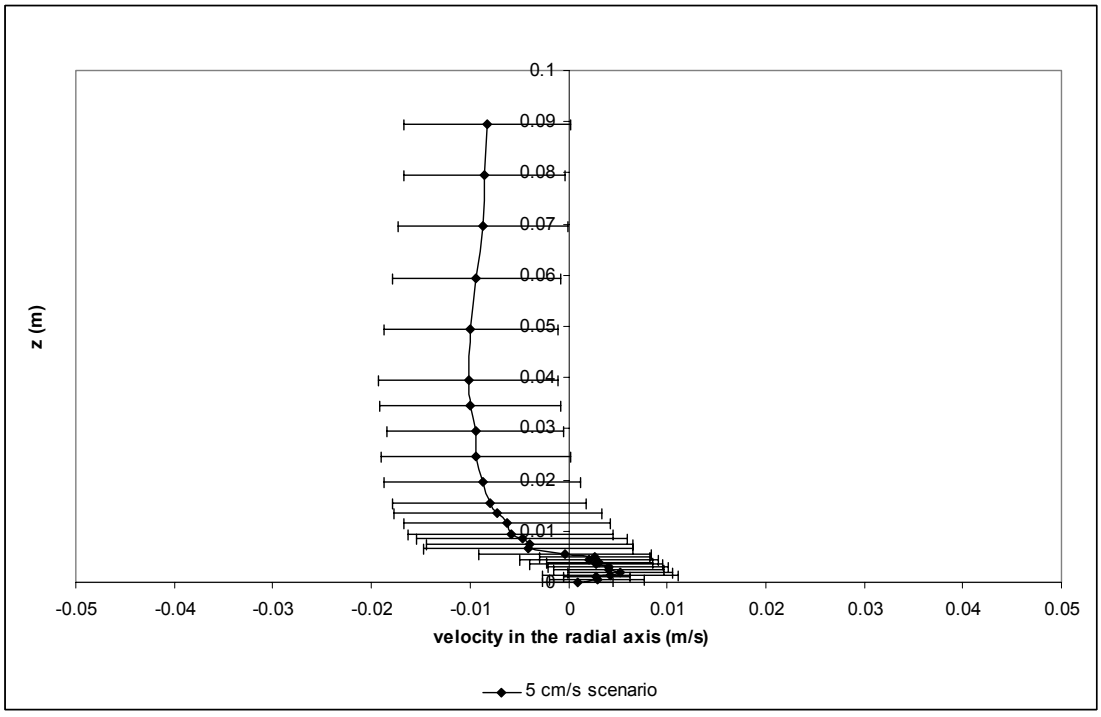

Figure 5 - Mean velocities along radial axis for the 5 cm/s scenario (error bars represent standard deviation)

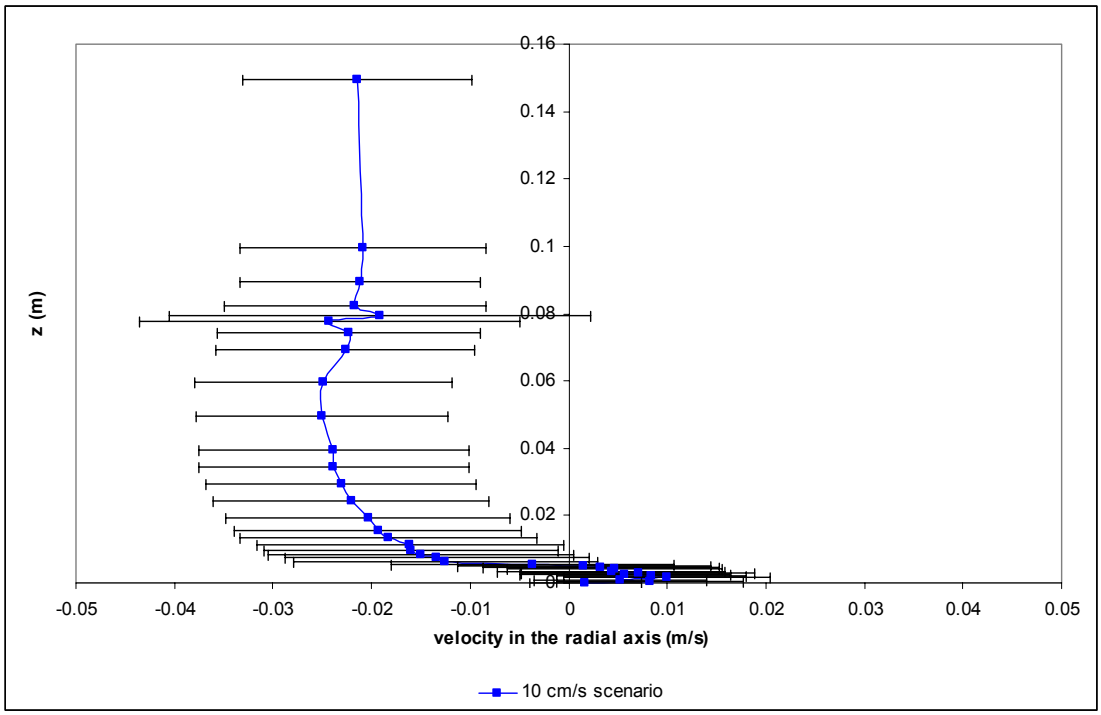

Figure 6 - Mean velocities along radial axis for the 10 cm/s scenario (error bars represent standard deviation)

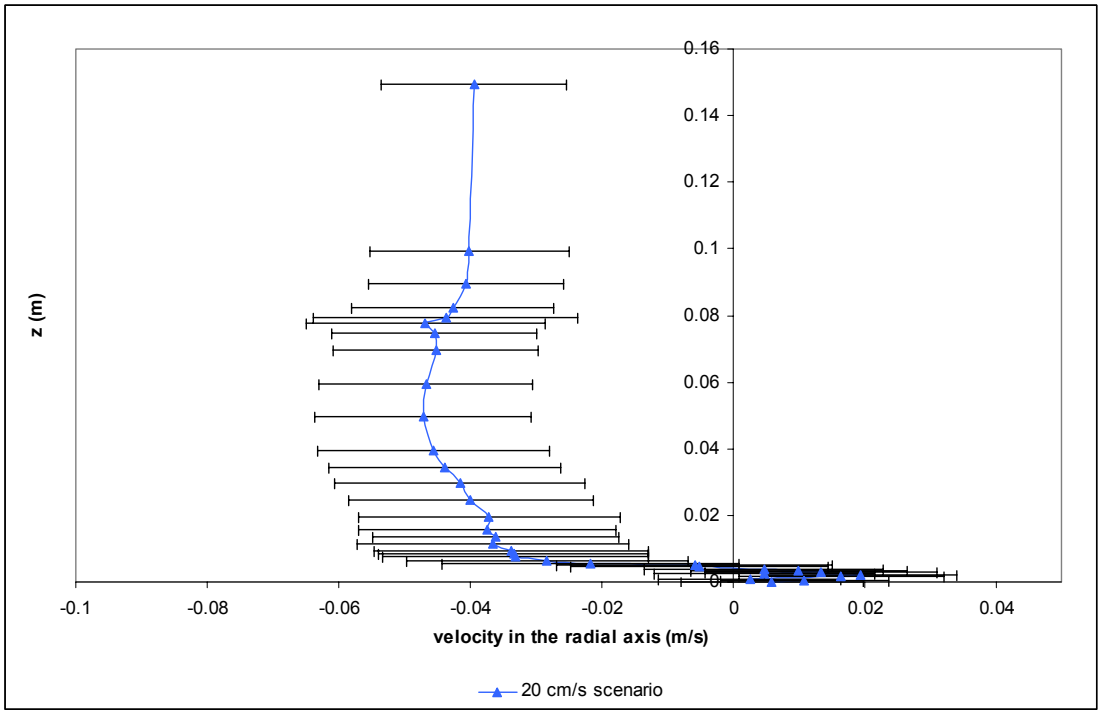

Figure 7 - Mean velocities along radial axis for the 20 cm/s scenario (error bars represent standard deviation)

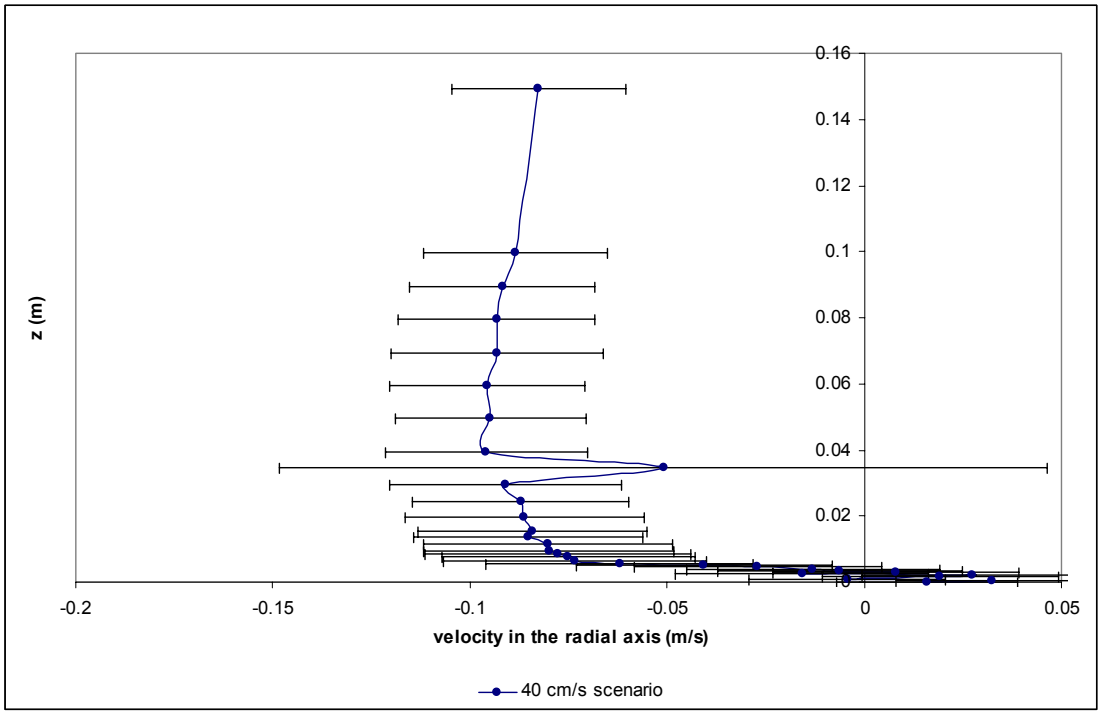

Figure 8 - Mean velocities along radial axis for the 40 cm/s scenario (error bars represent standard deviation)

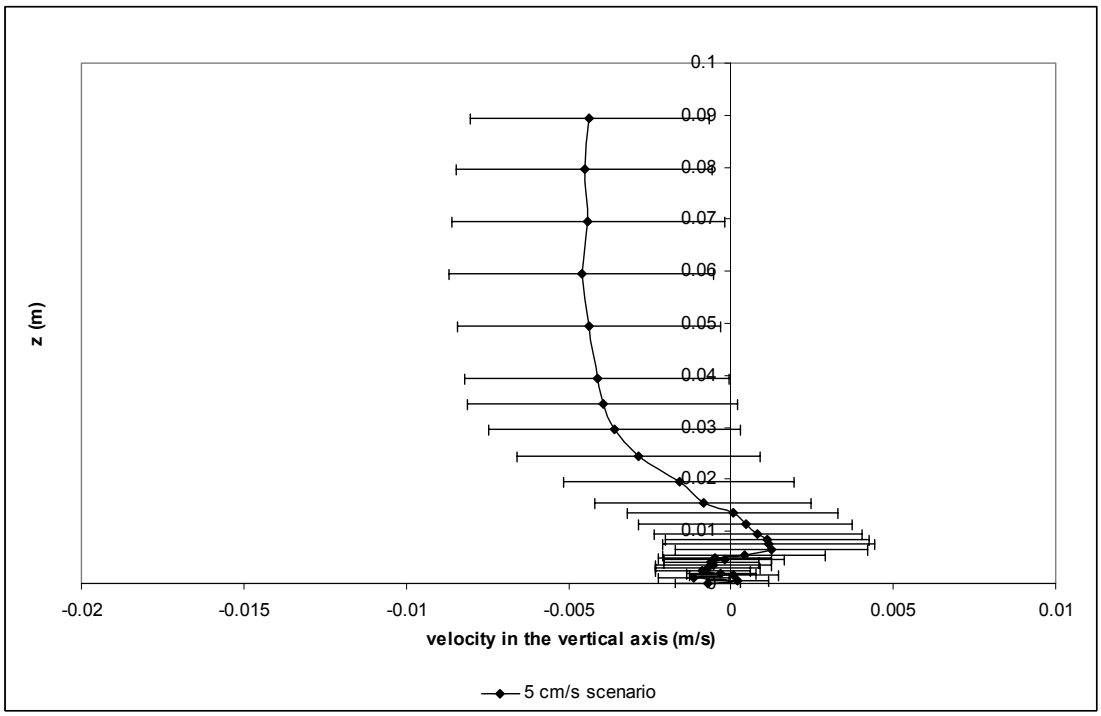

Figure 9 - Mean velocities along vertical axis for the 5 cm/s scenario (error bars represent standard deviation)

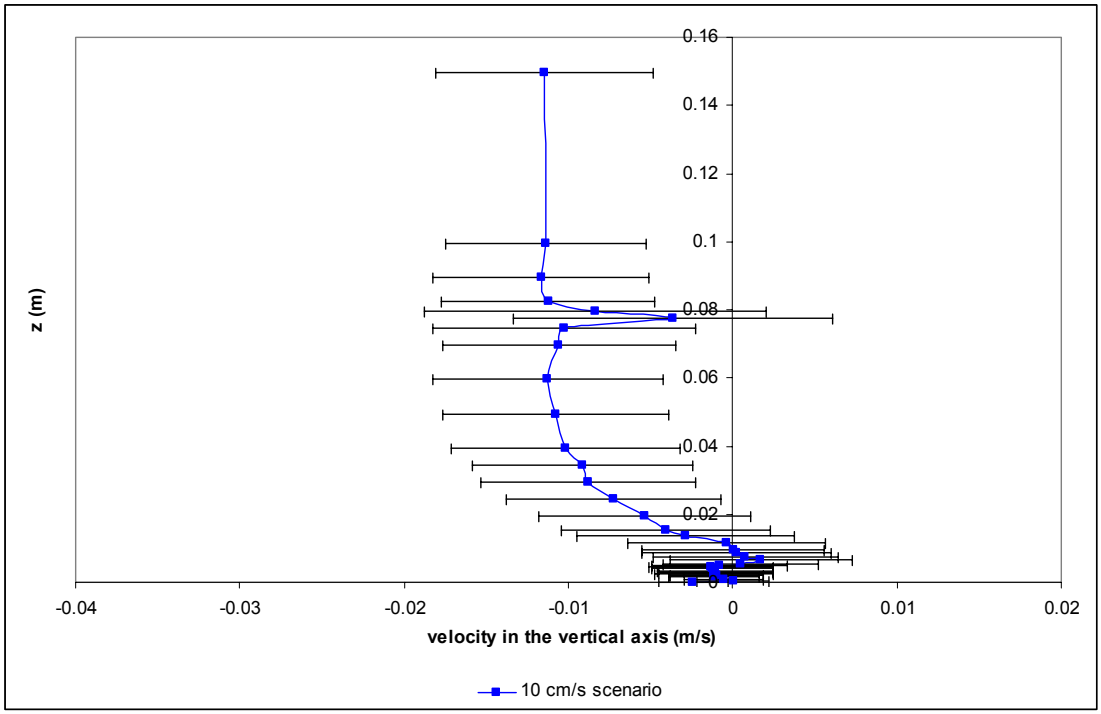

Figure 10 – Mean velocities along vertical axis for the 10 cm/s scenario (error bars represent standard deviation)

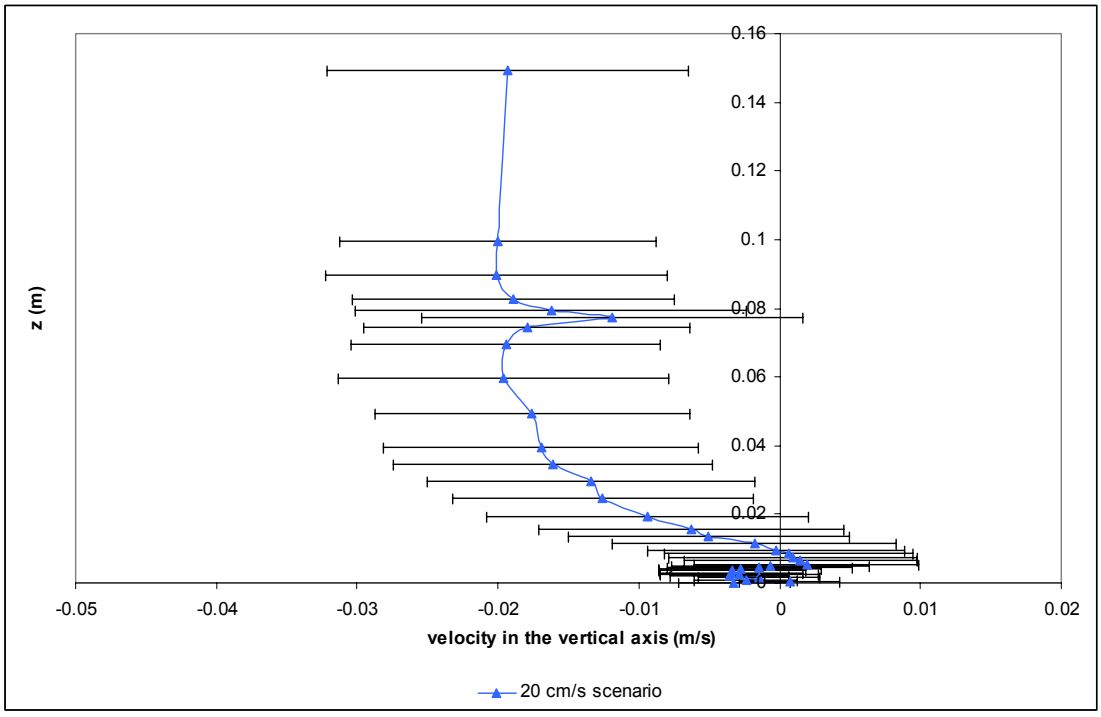

Figure 11 – Mean velocities along vertical axis for the 20 cm/s scenario (error bars represent standard deviation)

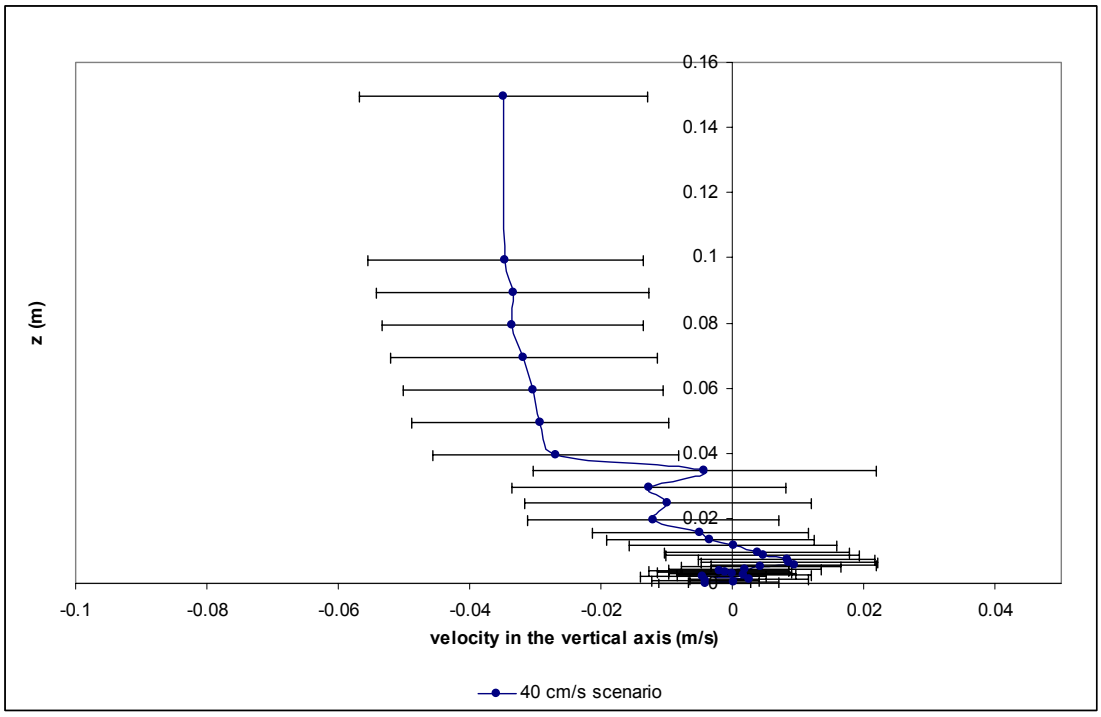

Figure 12 - Mean velocities along vertical axis for the 40 cm/s scenario (error bars represent standard deviation)

Modelling applications and results using MOHID

Model setup

MOHID is prepared to simulate annular flumes, using the following features:

- centrifugal acceleration inclusion in the inertial forces term when computing the hydrodynamic solution;
- use of circular horizontal discretization;
- use of cyclic boundary condition;

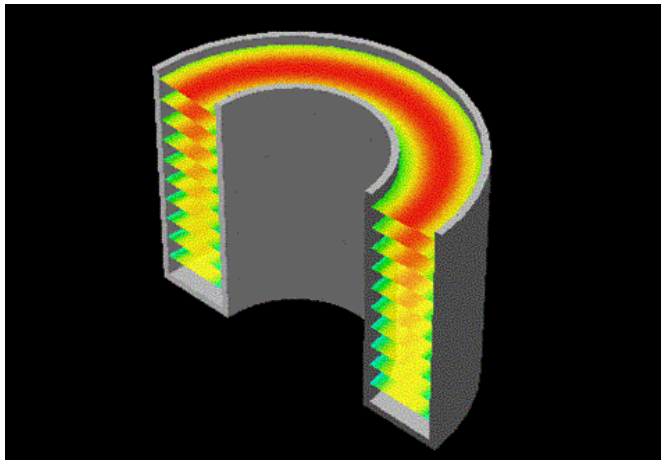

Figure 13 - 3D aspect of the flume design and vertical discrezation

Geometry parameters are input data that the user provides to the model. This means that the dimensions of the annular flume can be different in different simulations, just by introducing a different geometry parameters file. Nevertheless, all the simulations performed to test the model were applied with the dimensions of the annular flume operated in the laboratory (Table 1).

Water column height	32.5 cm
Exterior diameter	60 cm
Interior diameter	40 cm
Channel width	10 cm

Table 1 - Annular flume geometry parameters

Various discretizations were used, combining fine resolution with time step, having in mind the type of flow generated in this kind of domain. A horizontal discretization of 20x72 cells was used (Figure 14), with 40 layers vertical discretization using a sigma coordinate type.

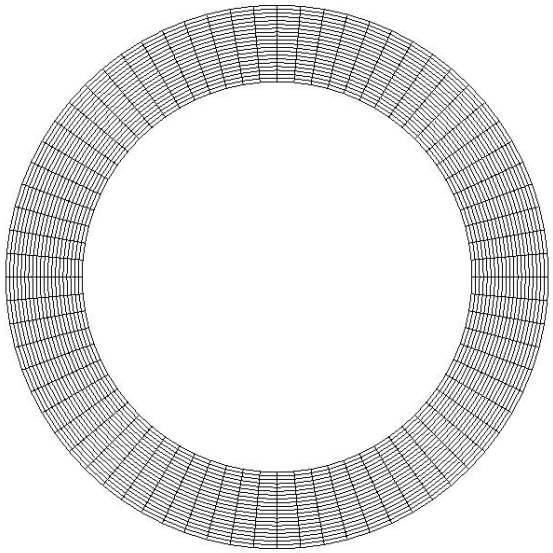

Figure 14 - Horizontal grid discretization

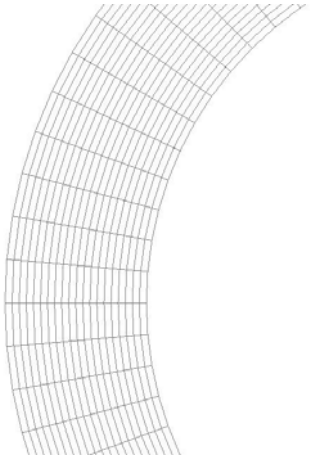

Figure 15 – Detail of horizontal grid discretization

Hydrodynamics solution is forced by applying a shear stress directly at the surface of the water column increasing linearly with the flume radius. This approach pretends to simulate the actual mechanism that forces water to flow in the annular flume operated in the lab. This is a rather fuzzy methodology to reproduce the actual mechanism used

in the annular channel, as MOHID does not support complex surface boundary conditions geometries, such as the mechanism used in the laboratory. This surface forcing provides momentum to the upper layer of the water column that by turbulent diffusion is transported to the lower layers and enables the water to speed up. The shear stress is imposed gradually in the beginning of the simulations, after what it remains constant enabling a steady state flow conditions to form. A non-slipping condition was considered to both the bottom and lateral boundaries, having the latter the most important contribution to the shear forces. Cyclic boundary conditions are considered, to assure continuous flow, both in the hydrodynamic module and in mass transport model.

Hydrodynamic results

Similarly to the scenarios created in the laboratory tests, MOHID was setup for four levels of velocity: 5, 10, 20 and 40 cm/s. This was done by applying different levels of shear stress at the water surface. Results are shown below, with correspondent comparisons with the ADV data measurements, for the 10 cm/s scenario.

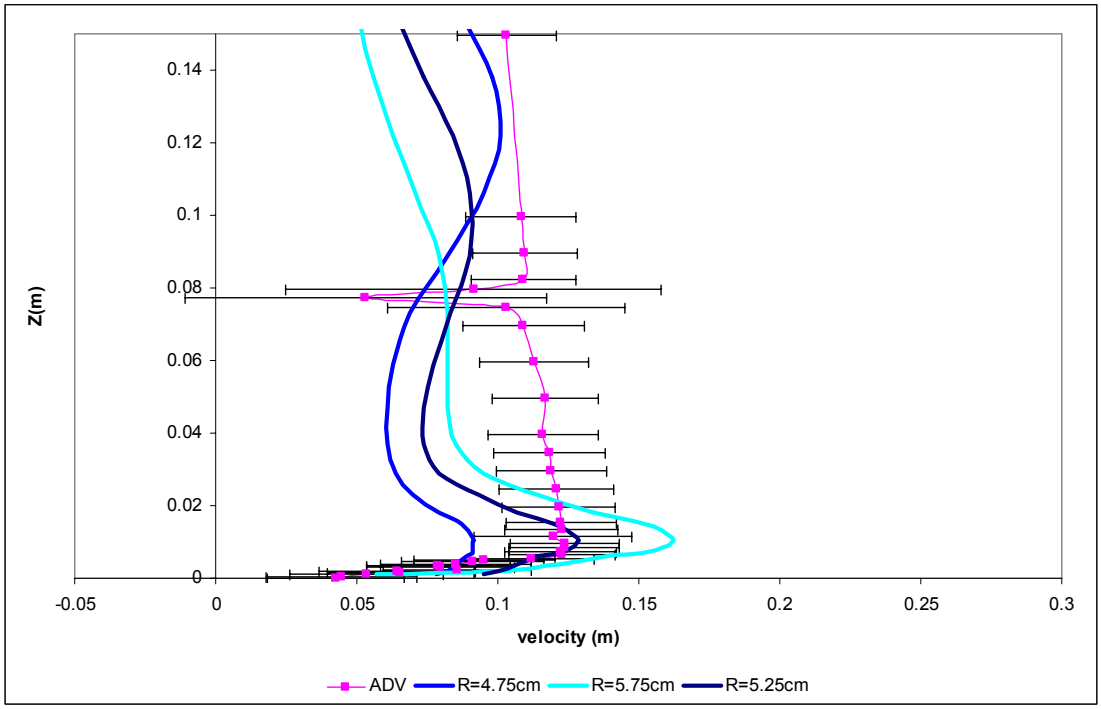

Figure 16 - Velocity along the rotation axis. Comparison between MOHID results and ADV data (10 cm/s scenario); 3 MOHID profiles are shown representing velocity variability along the axis, being the label correspondent to the distance in the radial axis from the interior wall.

In Figure 16 is presented a comparison between MOHID results and ADV results. ADV results are represented with standard deviation error bars. Note that due to the fact that there is some uncertainty regarding the exact position of the ADV in the centre of the channel section, 3 velocity profiles in the rotation direction produced by MOHID simulation are presented. As it can be seen, in a matter of 1 cm along the section, computed velocities can vary till almost 8 cm/s. Results cannot however reproduce the measured profile in totally but show good agreement in the bottom layers. However, in the just above layers the velocity is lower than the measurements, fact which is probably caused by a poor description of the system forcing scheme, namely through applying a shear stress at the water surface.

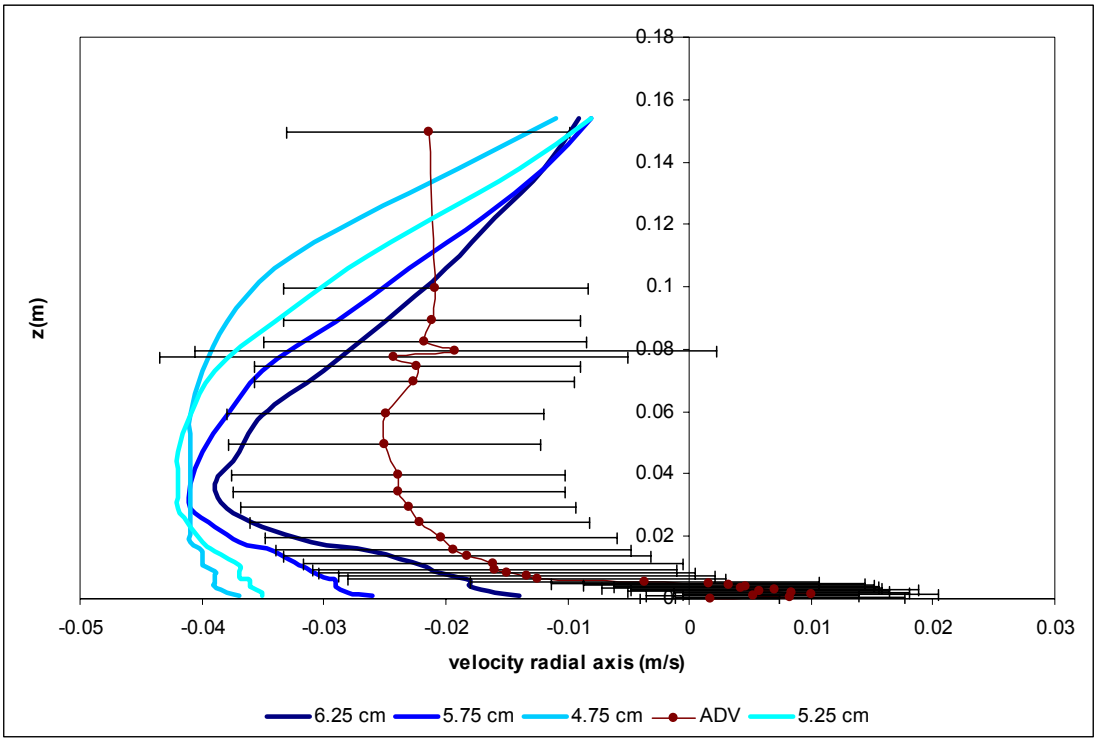

Figure 17 - Velocity along the radial axis. Comparison between MOHID results and ADV data (10 cm/s scenario); 4 MOHID profiles are shown representing velocity variability along the axis, being the label correspondent to the distance in the radial axis from the interior wall.

Figure 17 represents velocity comparisons with ADV data along the radial axis. As said before, the difference between laboratory and model results is probably due to surface boundary imposing. Nevertheless, qualitative agreement is found.

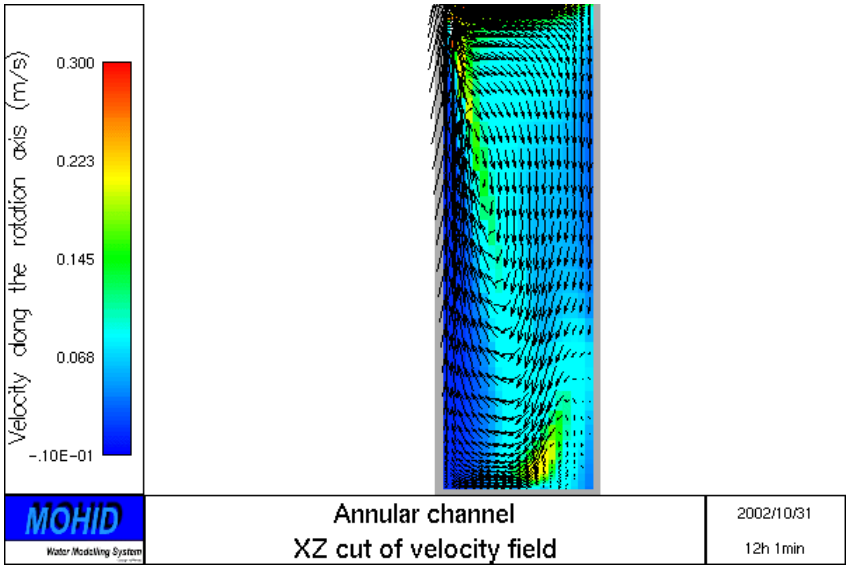

Figure 18 - Aspect of stabilized secondary flow simulated by MOHID (10 cm/s scenario)

Figure 18 shows a section cut of the annular channel representing the flow field velocities and (in colour) the velocity along the rotation axis. A secondary flow can be observed, as expected, due to the combination of both centrifugal forces and water level gradient.

Model applications using FLUENT

As the flow is axisymmetric, a 2D approach is possible and even recommended, so the number of calculation cells is reduced to a minimum. The simulations are lead first by the available experimental data. Four experiences were made with main stream velocities of 5, 10, 20 and 40 cm/s.

The simulations followed those steps:

- calibration: a steady simulation, with simplified boundary condition (VOF model), was run in order to determine the rotation velocity of the plate for which is obtained the corresponding main stream velocity
- unsteady simulation: after the calibration was made for the 40 cm/s case, an unsteady simulation was run with VOF model for free-surface modelling. Convergence to the steady case showed to be very slow. Moreover the results are quite similar to those produced by the initial (steady) simulation. So the steady simulation with no modelling of the free-surface seemed to be the best approach.
- steady simulations: once grid independence was shown, steady simulations were undertaken for the four cases with coarse grid to produce final results.

Calibration

Main stream velocity is not known a priori, so the idea is to simulate a simplified case, in order to approximate the velocity of the rotating plate.

In the simplified case, the free surface is substituted by a symmetry surface. This boundary condition which is often confused with periodic boundary condition states that:

- velocity component normal to the surface is equal to zero
- fluxes of any quantity through surface are also zero

Or,

$$\begin{cases} \vec{V} \cdot \vec{n} = 0 \\ \dfrac{\partial \phi}{\partial n} = 0 \end{cases}$$

It is, in fact, nothing less than what happens at a free surface, although in this case, the free surface is not allowed to deform.

The grid used is structured with 14078 nodes and refined near walls and in the region bellow the rotating plate (Figure 19*).

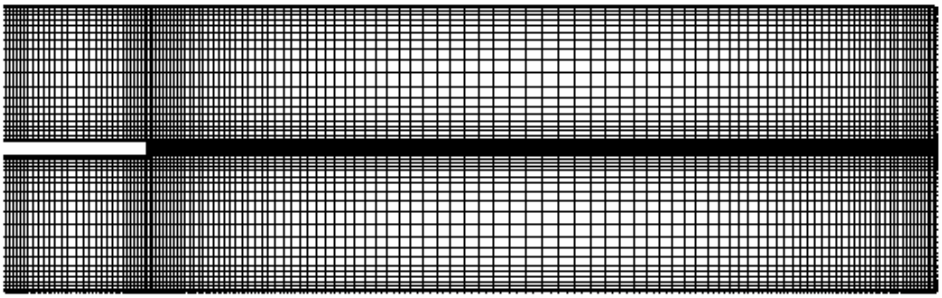

Figure 19 – Grid used in calibration phase

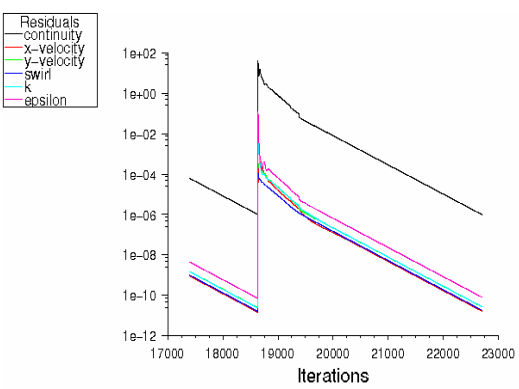

Figure 20 – Scaled residuals (steady simulation, v = 40cm/s)

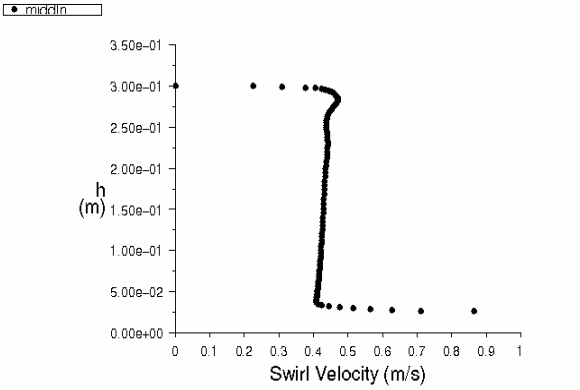

Figure 21 – Swirl velocity profile along section mid line (bottom is at h = 0.325m)

* N.B.: As it is represented, the channel appears laying on its side.

The idea is to run several simulations and reach iteratively a main stream velocity of 40 cm/s. An angular velocity of 68.8 rpm was finally found to produce the right velocity (Figure 21) and good convergence was achieved for residuals (Figure 20).

Unsteady Simulation

The unsteady calculation uses the VOF model for free surface. Due to the nature of the problem either the solution is steady, either periodic due to flow generated unsteadiness (e.g. vortex shedding). This is checked using some "probe" points where velocity is monitored. The upper boundary condition is a pressure outlet/inlet with pressure equal to atmospheric pressure.

Grid

The free surface deformation is captured using grid adaptation. Grid adaptation is a local refinement of the grid in zones of high gradient. The final grid can be seen on the next pictures (17759 nodes).

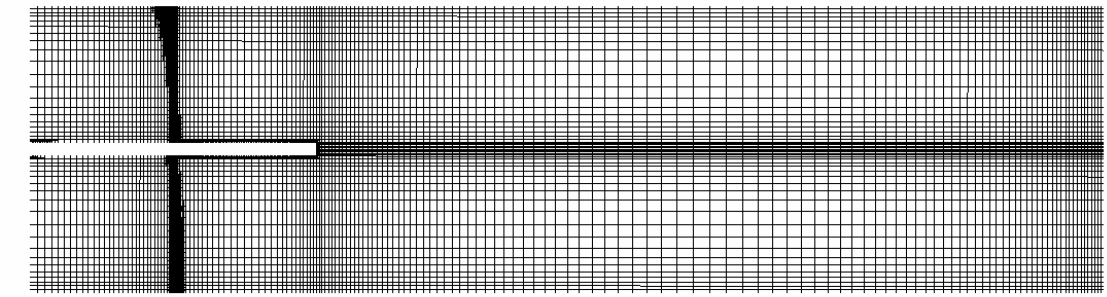

Figure 22 – Final grid for unsteady simulation after adaptation

The grid was refined near the wall and in the zone of water surface during the calculations. Grid adaptation produced 9560 additional nodes.

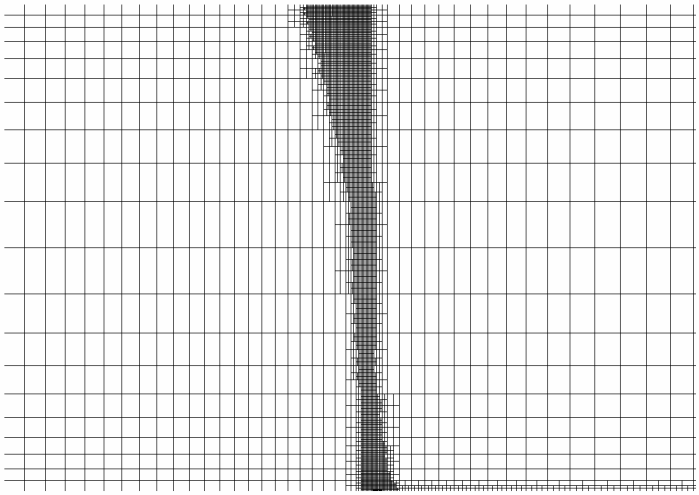

Figure 23 – Final grid for unsteady simulation after adaptation (detail)

This is from far the most costly calculation made in this study, but will show that steady calculations are sufficient to handle this case.

Results

In the following pictures we show water surface deformation and streamlines.

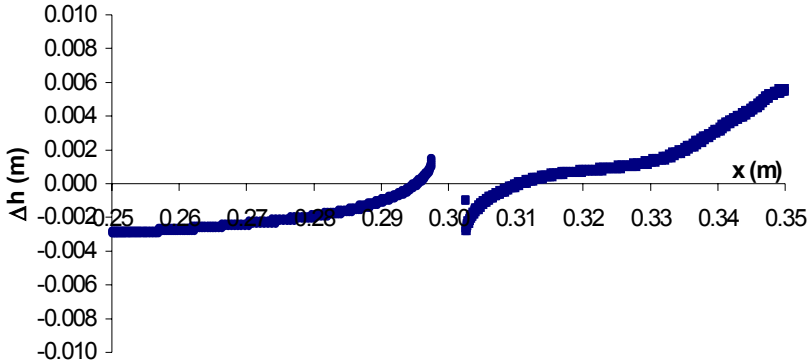

Figure 24 – Water surface profile (Δh: deviation to hydrostatic level)

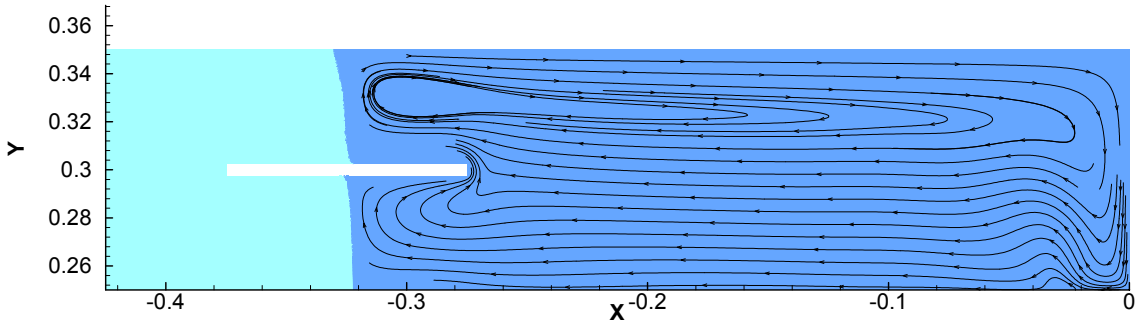

Figure 25 – Streamlines (figure is rotated 90º to the left) in the 40 cm/s scenario

Validity of the results

The step point when validating a numerical model is to look at the residuals to check convergence. As stated before, we should be around 10^{-6} for global mass imbalance.

Looking at the residuals for the last 1000 iterations, which correspond to 25 time steps, we see that, at each time step, the residuals converge to values clearly under the required. Worst values can be found for the continuity equation residuals that reach the 10^{-6}.

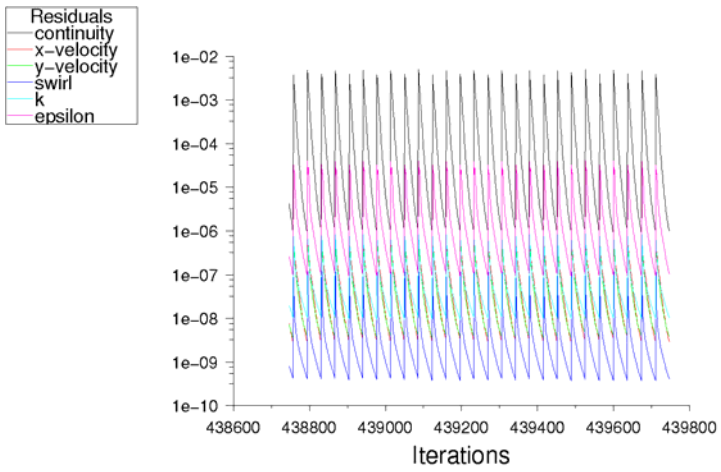

Figure 26 – Residuals (unsteady, v = 40cm/s)

This ensures convergence at each time step. However, if results converged to steady, the residuals should also converge to a given value, and it is not the case. An usual mean to check convergence is to take a look at the values of a certain quantity that is

variable with time, and observe its evolution. In Figure 27, we see swirl velocity at different locations as a function of time.

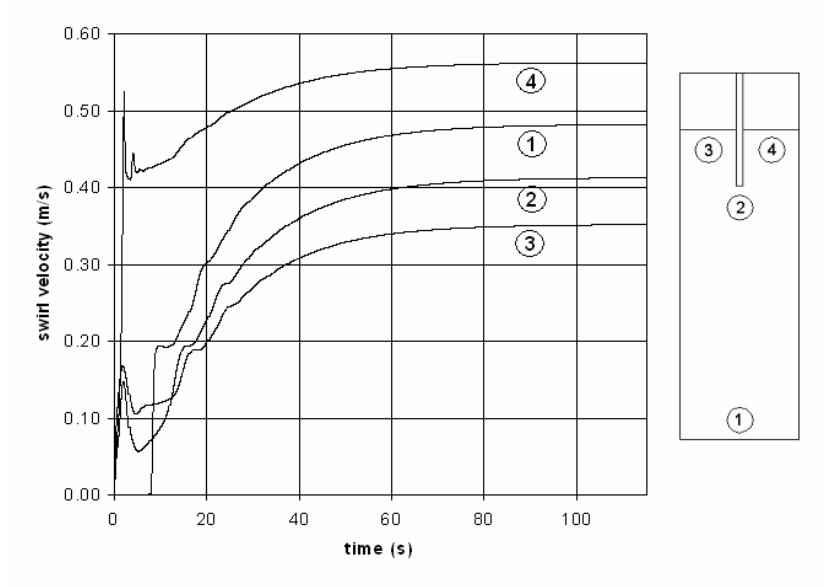

Figure 27 – Velocity along the rotation axis with time at different locations (v = 40cm/s)

At the end of the simulation, after 110s, the values tend to a fixed value. This shows convergence to steady state.

Finally, validation requires comparison with experimental measurements. The agreement between the two must be:

qualitative: numerical solution exhibits a pattern that is similar with the measurements (gradients and main structures of the flow are present)

quantitative: numerical solution gives results that are within a 15% error interval for local values

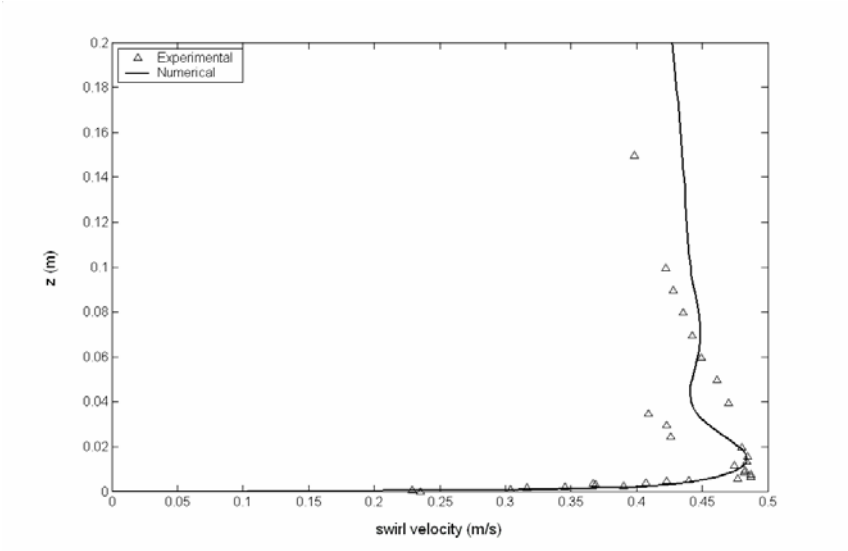

Figure 28 – Comparison with experimental data: velocity along the rotation axis (m/s)

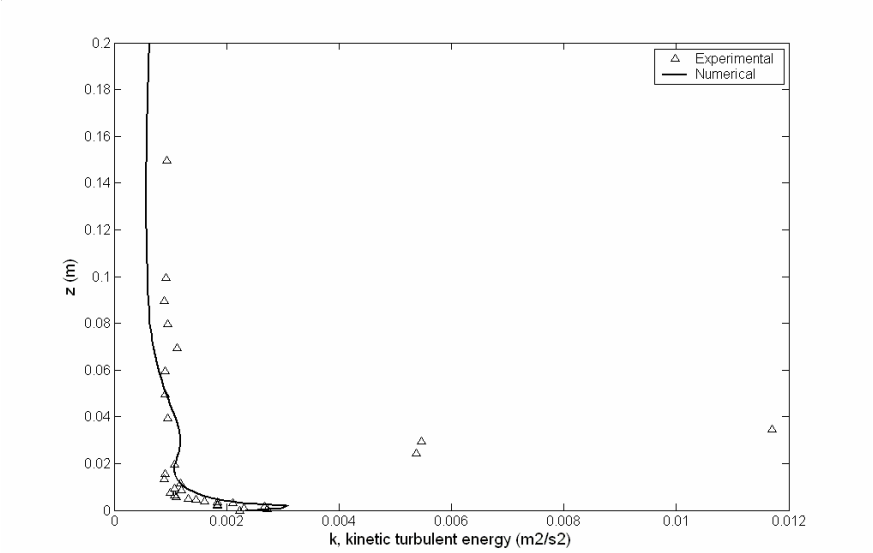

Figure 29 – Comparison with experimental data: kinetic turbulent energy along middle line

It can be seen in Figure 28 and Figure 29, where qualitative and quantitative agreement is found, except for three points in the second plot. It puts in evidence a known default of the k-ε model: its dissipation properties, that lead to an underestimation of turbulent quantities. Results shown in Figure 30 for axial velocity although not so clearly show consistency with laboratory data. Keeping in mind Figure 25, it is easier to understand the flow. At the bottom, the velocity is parallel to the wall and velocities near zero are expected. Then it should increase very fast in

absolute value with height. Indeed there is a high change in curvature in streamlines near the bottom. What data from experiment do not show is the inflexion point in the velocity graph that traduces also an inflexion point in the streamlines.

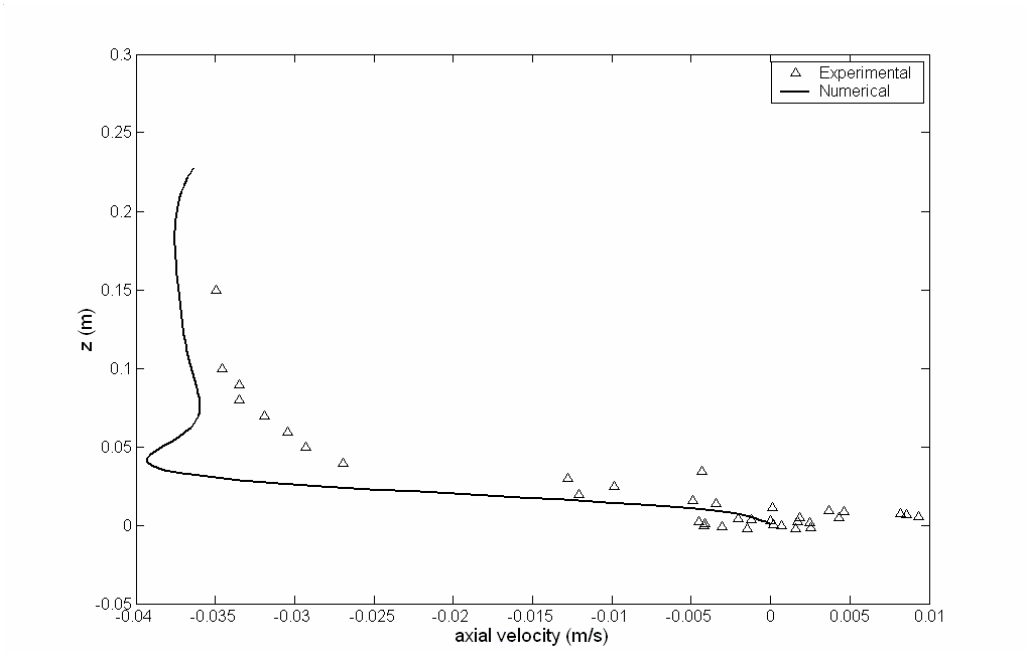

Figure 30 – Comparison with experimental data: vertical velocity (m/s)

The reason for this might be found in the following plot (Figure 31). It is by no means necessary to say that here, the agreement does not stand. But, fortunately, calculated velocities near the bottom are much higher than measured, hence we are being conservative in what concerns erosion. Looking again at Figure 25, we can see that streamlines form a closed bubble stretched in the vertical direction, laying against the exterior wall. This is a result of the presence of the plate conjugated with centrifugal force. According to the radial velocities measured, this bubble should not be so elongated. Above a certain height the radial velocity tend to zero for the numerical simulation. On the contrary, radial velocity has significant measured value. Therefore streamlines cannot be vertical as seen in the picture.

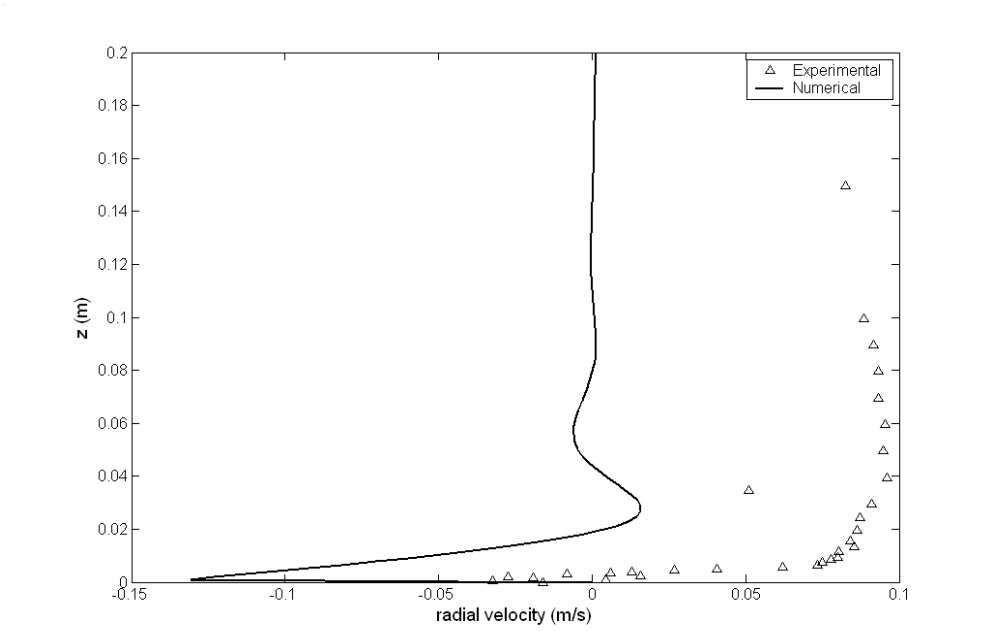

Figure 31 – Comparison with experimental data: radial velocity

Furthermore, a summary of all results produced by FLUENT model are presented.

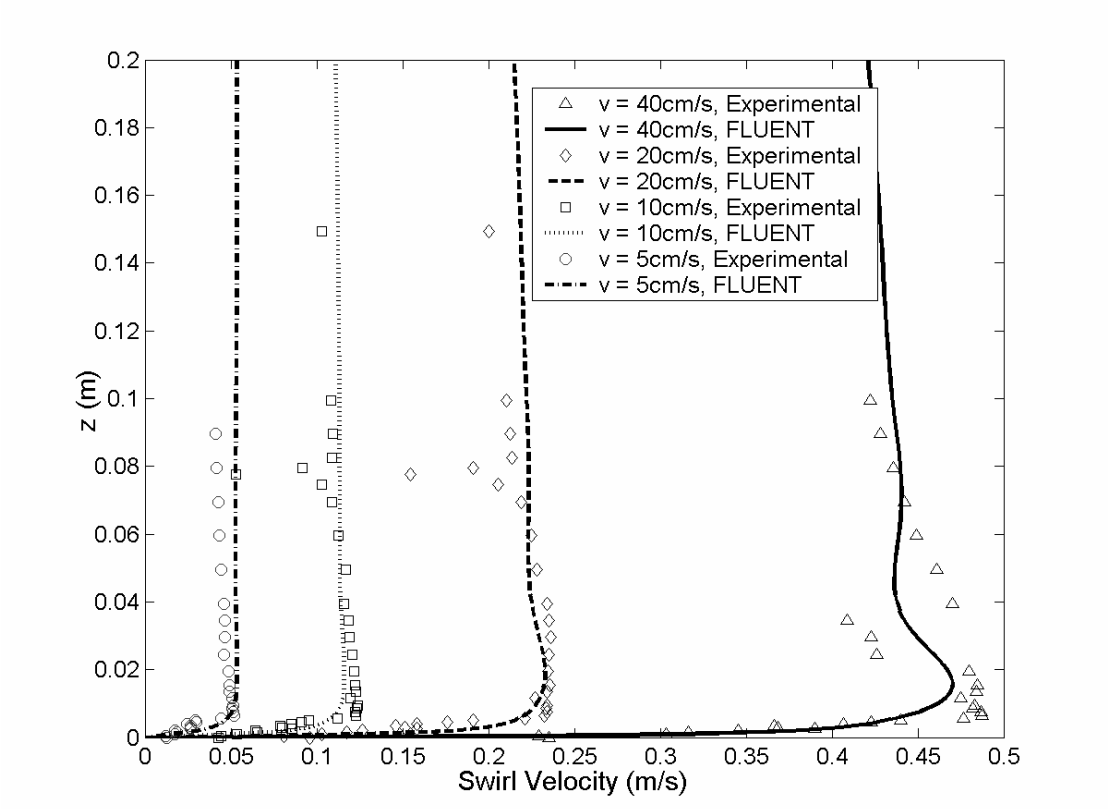

Figure 32 – Velocity in the rotation axis (m/s) ; Comparison between FLUENT and ADV data for the four scenarios.

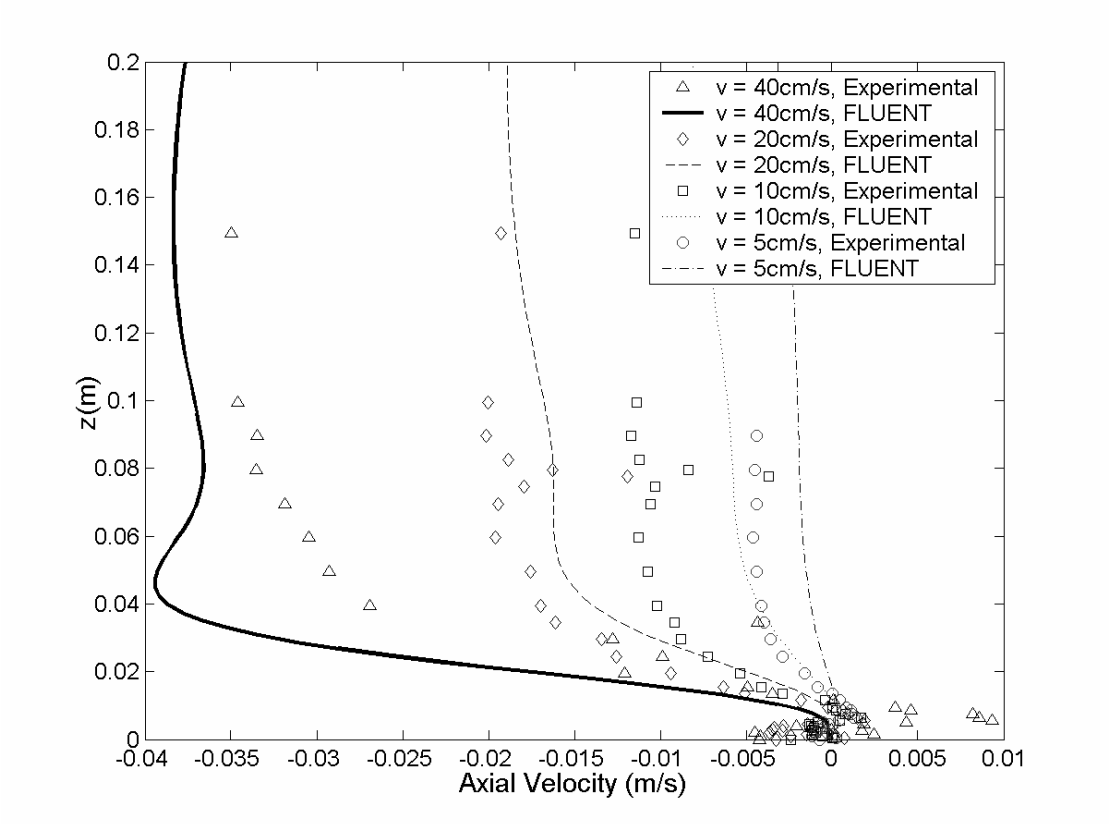

Figure 33 – Vertical velocity (m/s); Comparison between FLUENT and ADV data for the four scenarios.

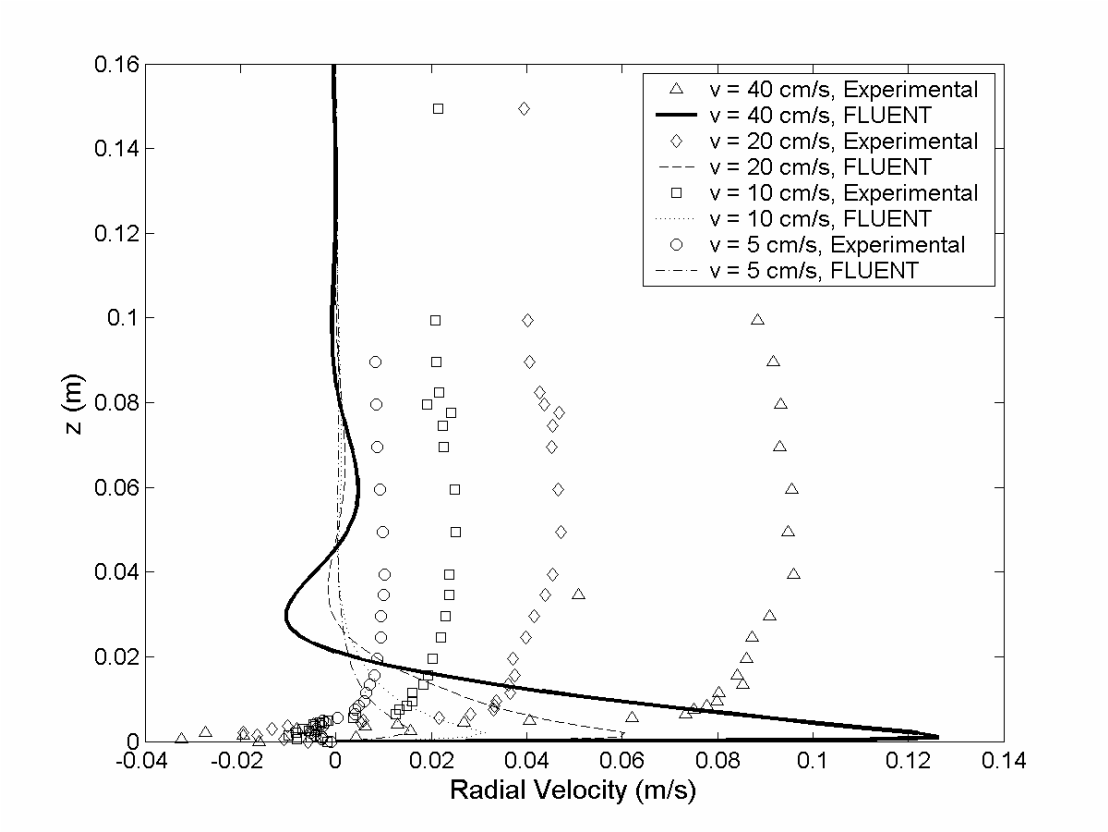

Figure 34 - Velocity in the radial axis (m/s); Comparison between FLUENT and ADV data for the four scenarios.

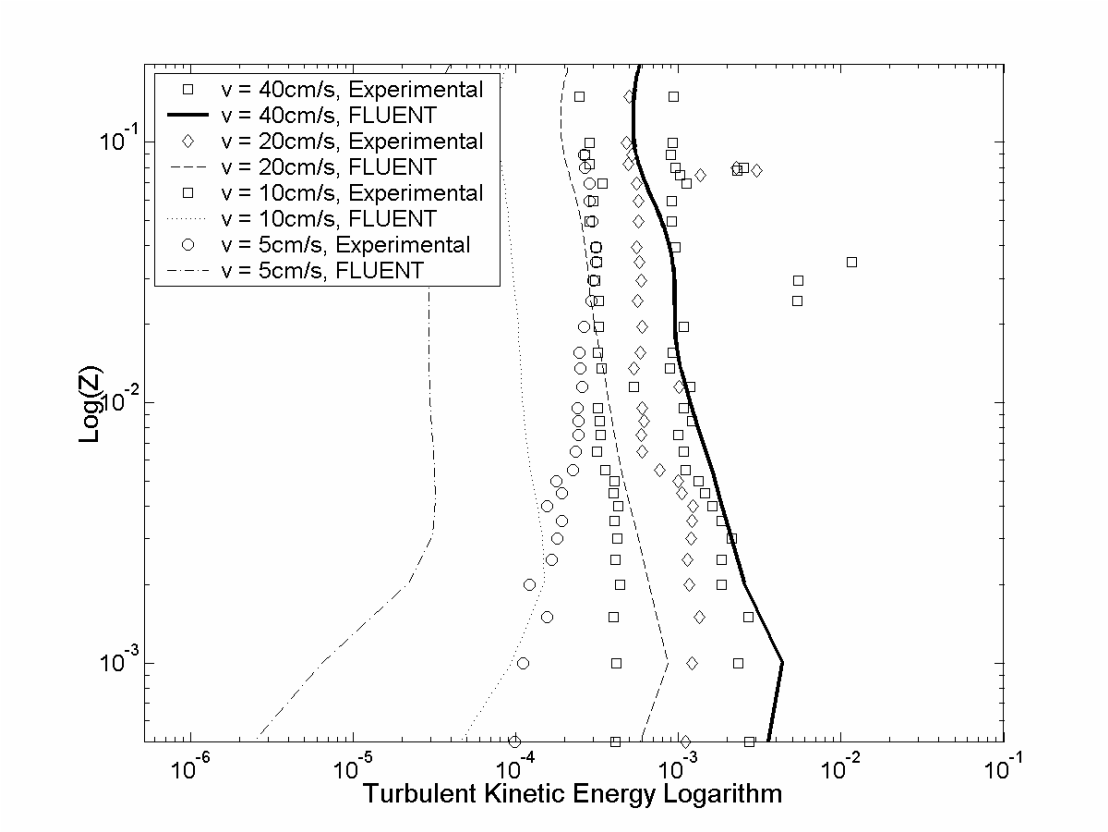

Figure 35 – Turbulent kinetic energy

As it can be observed it the figures above, FLUENT presents good agreement with ADV measured results, therefore being indicated to provide its solution to MOHID. FLUENT results can be introduced as input data to MOHID and from there profit from all the other potentialities of MOHID that FLUENT has, such as cohesive sediment transport and the possibility to simulate water quality processes, among others (as described in MOHID overview).

Main conclusions

The MOHID water modelling system is prepared to simulate water flow and cohesive sediment transport in an annular flume, therefore presenting to be an important numerical tool in this kind of studies, and particularly in the framework of this project.

Model results were compared with ADV data measurements performed in the annular channel. Two models were used, MOHID and FLUENT, the latter to serve as a reference to small applications to the first. MOHID, once calibrated, will be used to simulate laboratory studies on bioturbation and biodeposition. Simulations results were found satisfactory as one must understand the complex flow occurring in the annular channel, and by the fact that data measured with the ADV is not completely representative of the flow, as profiles were taken in only one point of the channel section (due to practical reasons, the ADV is fixed to the flume and can only be moved in the vertical axis). Better results agreement with measurements was found with FLUENT model results, but nevertheless, the secondary flow was difficult to simulate in its totality. Modelling results produced by FLUENT can be used to serve as flow field solution to MOHID, in order to provide a more accurate hydrodynamic solution, by means of an input file. This feature is currently being tested, and it can be used in further simulations. Nevertheless, surface boundary condition in MOHID will continue to be studied, in order to improve hydrodynamics results produced by MOHID in the annular channel applications.

Annexe 1: The hydrodynamic module

In this section the MOHID hydrodynamic module is described. The information flux of the hydrodynamic module, relative to the other modules of MOHID, is shown in Figure 0-1.

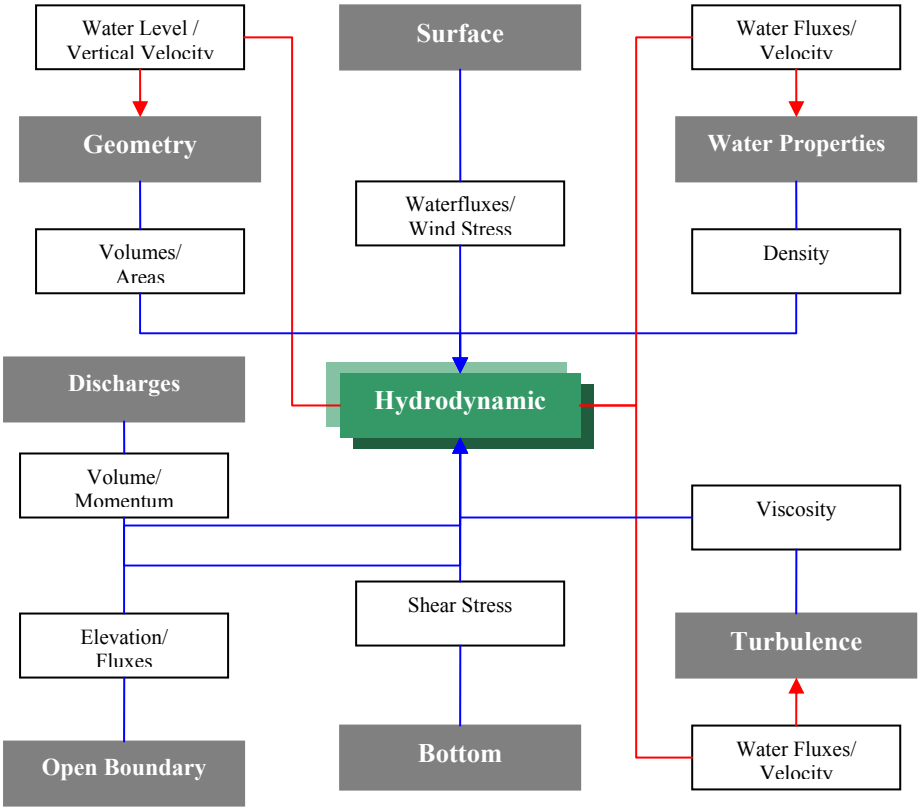

Figure 0-1: Information flux between the Hydrodynamic Module and other modules

Equations

The model solves the three-dimensional incompressible primitive equations. Hydrostatic equilibrium is assumed as well as Boussinesq and Reynolds approximations. All the equations below have been derived taken into account these approximations. The momentum balance equations for mean flow horizontal velocities are, in Cartesian form:

$$\partial_t u = -\partial_x(uu) - \partial_y(uv) - \partial_z(uw) + fv - \frac{1}{\rho_0}\partial_x p$$

$$+\partial_x\left((\nu_H+\nu)\partial_x u\right)+\partial_y\left((\nu_H+\nu)\partial_y u\right)+\partial_z\left((\nu_t+\nu)\partial_z u\right) \qquad \text{Eq. 0-1}$$

$$\partial_t v=-\partial_x(vu)-\partial_y(vv)-\partial_z(uw)-fu-\frac{1}{\rho_0}\partial_y p$$

$$+\partial_z\left((\nu_H+\nu)\partial_x v\right)+\partial_y\left((\nu_H+\nu)\partial_y v\right)+\partial_z\left((\nu_t+\nu)\partial_z v\right) \qquad \text{Eq. 0-2}$$

Where u, v and w are the components of the velocity vector in the x, y and z directions respectively, f the Coriolis parameter, ν_H and ν_t the turbulent viscosities in the horizontal and vertical directions, ν is the molecular cinematic viscosity (equal to 1.3 10^{-6} m^2 s^{-1}), p is the pressure. The temporal evolution of velocities (term on the left hand side) is the balance of advective transports (first three terms on the right hand side), Coriolis force (forth term), pressure gradient (next three terms) and turbulent diffusion (last three terms).

The vertical velocity is calculated from the incompressible continuity equation (mass balance equation):

$$\partial_x u+\partial_y v+\partial_z w=0 \qquad \text{Eq. 0-3}$$

by integrating between bottom and the depth z where w is to be calculated:

$$w(z)=\partial_x\int_{-h}^{z}u\,dx+\partial_y\int_{-h}^{z}v\,dy \qquad \text{Eq. 0-4}$$

The free surface equation is obtained by integrating the equation of continuity over the whole water column (between the free surface elevation η(x,y) and the bottom -h):

$$\partial_t\eta=-\partial_x\int_{-h}^{\eta}u\,dz-\partial_y\int_{-h}^{\eta}v\,dz \qquad \text{Eq. 0-5}$$

The hydrostatic approximation is assumed with:

$$\partial_z p+g\rho=0 \qquad \text{Eq. 0-6}$$

where g is gravity and ρ is density. If the atmospheric pressure p_{atm} is subtracted from p, and density ρ is divided into a constant reference density ρ_0 and a deviation ρ' from that constant reference density, after integrating from the free surface to the depth z where pressure is calculated, we arrive to:

$$p(z)=p_{atm}+g\rho_o(\eta-z)+g\int_{z}^{\eta}\eta\rho'\,dz \qquad \text{Eq. 0-7}$$

Eq. 0-7 relates pressure at any depth with the atmospheric pressure at the sea surface, the sea level and the anomalous pressure integrated between that level and the surface. By using this expression and the Boussinesq approximation, the horizontal pressure gradient in the direction x_i can be divided in three contributions:

$$\partial_{x_i} p = \partial_{x_i} p_{atm} - g\rho_0 \partial_{x_i} \eta - g\int_z \eta \partial_{x_i} \rho' dz \qquad \text{Eq. 0-8}$$

The total pressure gradient is the sum of the gradients of atmospheric pressure, of sea surface elevation (barotropic pressure gradient) and of the density distribution (baroclinic pressure gradient). This decomposition of the pressure gradient is substituted in Eq. 0-1 and Eq. 0-2.

The density is obtained from the salinity and from the temperature, which are transported by the water properties module.

Discretization

The spatial discretization is described in the geometry module. The temporal discretization is carried out by means of a semi implicit ADI (Alternate Direction Implicit) algorithm, introduced by Peaceman and Racford in 1955 (Fletcher, [1991]). This algorithm computes alternatively one component of horizontal velocity implicitly while the other is calculated explicitly. The resulting equation system is a tridiagonal one that can be solved by Thomas algorithm in an efficient and quick way. This allows preserving the stability advantages of implicit methods without the draw-backs of computational expensiveness and associated phase errors. A longer time-step can therefore be used. Two different discretizations are coded in the model: a 4 equations one with two time levels per iteration- the S21 scheme (Eq. 0-9) by Abbott et al. [1973]- and the 6 equation algorithm by Leendertsee, [1967], more convenient when intertidal zones are to be modelled, since velocities are updated every half time step. The S21 scheme is shown by Eq. 0-9:

$$\begin{aligned}
&\eta^{t+1/2}(u^{t+1}, u^{t}, v^{t+1/2}, v^{t-1/2}) \rightarrow u^{t+1} \rightarrow \\
&w^{*t+1/2} \xrightarrow{GeometryUpdate} w^{t+1/2} \rightarrow S^{t+1/2}, T^{t+1/2} \rightarrow \\
&\eta^{t+1}(u^{t}, u^{t+1}, v^{t+3/2}, v^{t+1/2}) \rightarrow u^{t+3/2} \rightarrow \\
&w^{*t+1} \xrightarrow{GeometryUpdate} w^{t+1} \rightarrow S^{T+1}, T^{T+1}
\end{aligned} \qquad \text{Eq. 0-9}$$

Each iteration is divided in two half steps. In the first half step, the free surface elevation η and then one of the horizontal velocities (u) are computed in an implicit way. The required value of the other velocity is taken from the previous time step. A vertical velocity w^* is computed from the continuity equation. Then, geometry is updated and the vertical velocity is corrected. The same process is followed in the next half step, but for the other component of horizontal velocity. In this diagram, salinity and temperature are computed each half step. As internal modes are much slower than external modes, S and T can be updated with a longer time step without losing accuracy and stability.

Discretization of the different processes

A sketch of the discretization will be given below. A full description of the discretization may be found in Martins, [2000] and Montero, [1999].

Free surface elevation is calculated by integrating the continuity equation (Eq. 0-3) over the whole water column. In the finite volume approach, this integration is done via a summation the volume fluxes over all water column cells. For the S21 discretization and the first half time step, it reads:

$$\frac{\eta_{ij}^{t+1/2}-\eta_{ij}^{t}}{\Delta t/2}=$$

$$\frac{1}{A_{hij}}\left[\frac{1}{2}\left(\sum_{kbot}^{k\max}U_{ijk}^{t+1}A_{u_{ijk}}^{t}+\sum_{kbot}^{k\max}U_{ijk}^{t}A_{u_{ijk}}^{t}\right)-\frac{1}{2}\left(\sum_{kbot}^{k\max}U_{ij+1k}^{t+1}A_{u_{ij+1k}}^{t}+\sum_{kbot}^{k\max}U_{ij+1k}^{t}A_{u_{ij+1k}}^{t}\right)\right]$$

$$+$$

$$\frac{1}{A_{hij}}\left[\frac{1}{2}\left(\sum_{kbot}^{k\max}V_{ijk}^{t+1/2}A_{v_{ijk}}^{t}+\sum_{kbot}^{k\max}U_{ijk}^{t-1/2}A_{v_{ijk}}^{t}\right)-\frac{1}{2}\left(\sum_{kbot}^{k\max}V_{i+1jk}^{t+1/2}A_{u_{i+1jk}}^{t}+\sum_{kbot}^{k\max}U_{i+1jk}^{t-1/2}A_{u_{i+1jk}}^{t}\right)\right] \quad \text{Eq. 0-10}$$

where $A_{hij}=DUX_{ij}*DVY_{ij}$ is the area projected on the horizontal plane. Fluxes are temporally averaged, so the calculus is centered in t+1/2. An analogous discretization is carried out for the next half step. The fluxes $U{\cdot}AU$ and $V{\cdot}AV$ are obtained from the momentum equation. The discretization of the different terms will be discussed below.

If we discretize equation (Eq. 0-1) making use of and S21 discretization, we arrive to (an equivalent equation is derived for v, Eq. 0-2) for every cell u_{ijk} of the grid:

$$\frac{\Omega^t_{u_{ijk}}(U^{t+1}_{ijk} - U^t_{ijk})}{\Delta t} + \sum_{m=1}^{Nfaces} \vec{F}\,\vec{n}\,A_m = f_{u_{ijk}}\,\Omega^t_{u_{ijk}}\,\overline{V}^t_{ijk} \qquad \text{Eq. 0-11}$$

where $\Omega^t{}_{Uijk}$ is the volume of the computation cell for U_{ijk} and f_{uijk} is the value of the Coriolis parameter for that cell. The value $V,\overline{\ }^t_{ijk}$ represents the average value of the v-component of the flow on this cell. The second term on the left hand side represents the fluxes of the forces F_m through the surface A_m of the cell m. The Coriolis force is the term on the right hand side and the other terms in the equation are included in the summation on the left hand side.

Coriolis term

As we can see on the right hand side of Eq. 0-11, the Coriolis term is discretized explicitly, although it is well-known that this implies a restriction on Δt ($\Delta t \leq 2/f$, with f the Coriolis parameter). This limitation is not critical for coastal applications -for latitude of 43º Δt $\leq$2000 s $\approx$ 5h 30min, that is much bigger than the time steps chosen in these applications.

The other terms in this formulation are seen as fluxes through the surfaces of the control volume, and therefore enter in the second term on the left hand side.

Advective terms

In order to guarantee momentum conservation, fluxes into the element must have null divergence. This is accomplished by using in the convective terms the same fluxes obtained in the last computation of elevation and vertical velocity. Convective fluxes are computed in every face of the cell:

$$-\sum_{m=1}^{Nfaces} \vec{F}_m \cdot \vec{n}\,A_m = \Big[(U \cdot ufluxU)^t_{ij+1k} - (U \cdot ufluxU)^t_{ijk} + (U \cdot ufluxV)^t_{i+1jk} - (U \cdot ufluxV)^t_{ijk} + (U \cdot ufluxW)^t_{ijk+1} - (U \cdot ufluxW)^t_{ijk}\Big] \qquad \text{Eq. 0-12}$$

with $ufluxU_i$ denotes the flux of U_i through the cell of calculus of u. A mixed scheme upwind-central differences is used for computing $ufluxU_i$ (James, [1987], Santos

[1995]). Horizontal advective fluxes are discretized explicitly as the restriction that surface waves impose on stability is small for the characteristic range of velocities. The vertical advective term can give problems if the layer thickness is small, as can happen in shallow zones with sigma grids. Two solutions to this problem have been introduced in the model: an implicit discretization or neglecting this term in those regions.

Barotropic pressure gradient

The restriction of surface waves on stability lead to the implementation of the semi-implicit algorithm so this term limits stability and consequently is discretized implicitly. For the cell u_{ijk} and the first semi-step:

$$-\sum_{m=1}^{Nfaces} \vec{F}_m \cdot \vec{n} A_m = \frac{1}{\rho_0}\left[(P_{atm_{ij-1}}^{t+1/2} - P_{atm_{ij}}^{t+1/2}) + \rho_0 g(\eta_{ij-1}^{t+1/2} - \eta_{ij}^{t+1/2})\right] A_{u_{ijk}}^t \qquad \text{Eq. 0-13}$$

This expression, when substituted in the equation for the free surface, results in a tridiagonal system, which is solved by Gaussian elimination. In the equation for velocities, the values of η are already known, which allows the explicit discretization of this term for introduction in momentum equations.

Baroclinic pressure gradient

Internal modes do not introduce a stringent restriction on stability, so they can be discretized explicitly. The fluxes induced by this term through the faces of a uijk cell are:

$$-\sum_{m=1}^{Nfaces} \vec{F}_m \cdot \vec{n} S_m = \frac{g}{\rho_0}\left(\sum_{l=k+1}^{k\max}(\rho'^t_{ij-1l} DWZ_{ij-1l}) + \rho'^t_{ij-1k}\Delta z^t_{ij-1k}\right) A_{u_{ijk}}^t$$
$$-\left(\sum_{l=k+1}^{k\max}(\rho'^t_{ijl} DWZ_{ijl}) + \rho'^t_{ijk}\Delta z^t_{ijk}\right) A_{u_{ijk}}^t \qquad \text{Eq. 0-14}$$

where Δz^t_{ijk} represents the vertical distance from the cell top to the velocity point and arises as a consequence of the vertical staggering of the grid (ρ' is not defined in the same point as the u-velocity).

Horizontal diffusive fluxes

Horizontal diffusive fluxes are computed in every vertical face of the cell, applying that fluxes are normal to these faces:

$$-\sum_{m=1}^{Nfaces} \vec{F}_m \cdot \vec{n}\, A_m = (F^t_{ij-1/2k}\, Azx^t_{ij-1k} - F^t_{ij+1/2k}\, Azx^t_{ijk}) +$$

$$(F^t_{i-1/2jk} \frac{Av^t_{ijk} + Av^t_{ij-1k}}{2} - F^t_{i+1/2jk} \frac{Av^t_{i+1jk} + Av^t_{i+1j-1k}}{2}) \qquad \text{Eq. 0-15}$$

Fluxes for x direction are:

$$F_{ij-1/2k} = \nu^t_{H_{ij-1k}} \frac{U^t_{ijk} - U^t_{ij-1k}}{DUX_{ij-1}} \qquad \text{Eq. 0-16}$$

and for the y-direction:

$$F_{i-1/2jk} = \nu^t_{H_{i-1/2j-1/2k}} \frac{U^t_{ijk} - U^t_{ij-1k}}{(DYY_{ij} + DYY_{i-1j})/2} \qquad \text{Eq. 0-17}$$

where the horizontal viscosity coefficient v^t_H is interpolated to the appropriate point.

Vertical diffusion

These terms must be discretized implicitly as the restriction imposed by an explicit discretization on the time step is strict for the resolution we will use.

$$-\sum_{m=1}^{Nfaces} \vec{F}_m \cdot \vec{n}\, A_m = (F^{t+1}_{ijk-1/2} - F^{t+1}_{ijk+1/2}) A^t_{h_{ij-1/2}}) + \qquad \text{Eq. 0-18}$$

with fluxes given by the equation:

$$F^{t+1}_{ijk-1/2} = \nu^t_{ij-1/2k-1} \frac{U^{t+1}_{ijk} - U^{t+1}_{ijk-1}}{DUZ^t_{ijk-1}} \qquad \text{Eq. 0-19}$$

Free surface boundary condition

All advective fluxes across the surface are assumed to be null. This condition is imposed by assuming that the vertical flux of W at the surface is null:

$$Wflux\big|_{surface} = 0 \qquad \text{Eq. 0-20}$$

Diffusive flux of momentum is imposed explicitly by means of a wind surface stress, τw:

$$\nu \frac{\partial \overline{v_H}}{\partial z}\Big|_{surface} = \vec{\tau}\, w \qquad \text{Eq. 0-21}$$

Wind stress is calculated according to a quadratic friction law:

$$\vec{\tau w} = C_D \rho_a \vec{W} \left| \vec{W} \right| \qquad \text{Eq. 0-22}$$

where C_D is a drag coefficient that is function of the wind speed, ρ_a is air density and W is the wind speed at a height of 10 m over the sea surface.

Bottom boundary condition

Also at the bottom, advective fluxes are imposed as null and diffusive flux of momentum is estimated by means of a bottom stress that is calculated by a non-slip method with a quadratic law that depends on the near-bottom velocity. So, the diffusive term at the bottom is written as:

$$\nu \frac{\partial \vec{v}_H}{\partial z}\Big|_{bottom} = C_D \vec{v}_H \left| \vec{v}_H \right| \qquad \text{Eq. 0-23}$$

C_D is the bottom drag coefficient that is calculated with the expression:

$$C_D = \left(\frac{\kappa}{\log\left(\frac{z + z_0^b}{z_0^b} \right)} \right)^2 \qquad \text{Eq. 0-24}$$

where κ is von Karman constant and z^b_0 is the bottom roughness length. This quadratic law is derived from the logarithmic law of the wall near boundaries characteristic of boundary layers, as the bottom velocities are located half a grid box above the bottom. This term is calculated semi-implicitly following Backhaus [1985] for the sake of numerical stability.

No fluxes of salinity and temperature are considered at the bottom.

Lateral closed boundaries

At these boundaries, the domain is limited by land. For the resolution we are using, this lateral boundary layer is resolved, so an impermeable, free slip condition can be used:

$$\frac{\partial \vec{v}_H}{\partial \eta} = 0 \qquad \text{Eq. 0-25}$$

$$\vec{v} \cdot \vec{n} = 0 \qquad \text{Eq. 0-26}$$

In the finite volume formalism, these conditions are implemented straightforwardly by specifying zero normal water fluxes and zero momentum diffusive fluxes at the cell faces in contact with land.

Open boundaries

Open boundaries arise from the necessity of confining the domain to the region of study. The values of the variables must be introduced there such that it is guaranteed that information about what is happening outside the domain will enter the domain in a way that the solution inside the domain is not corrupted. Also, waves generated inside the domain should be allowed to go out. There exists no perfect open boundary condition and the most suitable would depend on the domain and the phenomena to be modelled. A recent review paper comparing open boundary conditions in test cases can be found in Palma and Matano [1999]. Some different open boundaries are already introduced in MOHID 3D (Santos, [1995], Montero, [1999]) and some others like FRS (Flow Relaxation Scheme) are in progress.

Moving boundaries

Moving boundaries are closed boundaries that change position in time. If there are inter tidal zones in the domain, some points can be alternatively covered or uncovered depending on tidal elevation. A stable algorithm is required for modelling these zones and their effect on hydrodynamics of estuaries. A detailed exposition of the algorithms used in MOHID can be found in Martins et al. [1999] and Martins [1999].

References

Abbott, M.B., A. Damsgaardand and G.S. Rodenhuis (1973) - System 21, Jupiter, a design system for two dimensional nearly horizontal flows. J. Hyd. Res, 1, 1-28

Backhaus, J (1985) - A three dimensional model for the simulation of shelf sea dynamics. Dt. Hydrogr.Z., 38, 165-187.

Braunschweig, F (2001) – Generalização de um modelo de circulação costeira para albufeiras, MSc. Thesis, Instituto Superior Técnico, Technical University of Lisbon

C. Schweim, et al., Large Eddy Simulation of a Lid-Driven Rotating Annular Flume Flow, presented on the 4th International Conference on Hydroinformatics Iowa, 23/27 July 2000

Cancino, L. and R. Neves (1999) - Hydrodynamic and sediment suspension modelling in estuarine systems. Part II: Application to the Western Scheldt and Gironde estuaries, Journal of Marine Systems 22, 117-131

Croft N., Unstructured Mesh – Finite Volume Algorithms for Swirling, Turbulent Reacting Flows, Ph.D. Thesis, The University of Greenwich, April 1998

Fletcher, C.A.J. (1991) - Computational techniques for fluid dynamics. Volume I. 2nd Edition. Springer Series in Computational Physics, Springer Verlag, 401 pp., New York

James, I.D. (1987) - A general three-dimensional eddy-resolving model for stratified seas. In: Three-dimensional models of marine and estuarine dynamics,edited by J.C.Nihoul and B.M.Jamart, Elsevier Oceanography Series 45 Amsterdam, 1-33

Leendertsee, J.J. (1967) - Aspects of a computational model for long water wave propagation. Rand Corporation, Memorandum RM-6230-RC, Santa Monica, 1970.

Leitão, P. C. (1996) – Modelo de Dispersão Lagrangeano Tridimensional. Ms. Sc. Thesis, Universidade Técnica de Lisboa, Instituto Superior Técnico

Martins, F. (1999) – Modelação Matemática Tridimensional de Escoamentos Costeiros e Estuarinos usando uma Abordagem de Coordenada Vertical Genérica. Ph. D, Thesis, Universidade Técnica de Lisboa, Instituto Superior Técnico

Martins, F., P. Leitão, A. Silva and R. Neves (2000) - 3D modeling in the Sado estuary using a new generic vertical discretization approach, submitted to Oceanologica Acta

Montero, P. (1999) - Estudio de la hidrodinámica de la Ría de Vigo mediante un modelo de volúmenes finitos (Study of the hydrodynamics of the Ría de Vigo by means of a finite volume model), Ph.D. Dissertation, Universidad de Santiago de Compostela, in Spanish

Montero, P., M. Gómez-Gesteira, J. J. Taboada, M. Ruiz-Villarreal., A. P. Santos, R. J. J. Neves, R. Prego and V. Pérez-Villar (1999) - On residual circulation of Vigo Ría using a 3D baroclinic model, Boletín Instituto Español de Oceanografía,,n o 15. SUPLEMENTO-1

Neves, R., H. Coelho, P. Leitão, H. Martins, and A. Santos (1998) - A numerical investigation of the slope current along the western European margin. In: Burgano V.,

Palma, E. and R. P. Matano (1998) - On the implementation of passive open boundary conditions for a general circulation model: The barotropic mode. Journal of Geophysical Research, 103, 1319-1342

Pérez-Villar, V. (1999) - ''Ordenación Integral del Espacio Maritimo-Terrestre de Gali-cia: Modelización informática'' (Integrated Management of the Galician Maritime-Terrestrial Space: Numerical Modelling). Final report by the Grupo de Física Non Lineal, Consellería de Pesca, Marisqueo e Acuicultura. Xunta de Galicia.

Pina, P. M. N (2001) – An Integrated Approach to Study the Tagus Estuary Water Quality. MSc Thesis, Universidade Técnica de Lisboa, Instituto Superior Técnico

Pope S.B., Turbulent Flows, Cambridge, 2000

Santos, A. J. (1995) - Modelo Hidrodinâmico Tridimensional de Circulação Oceânica e Estuarina. Ph. D, Thesis, Universidade Técnica de Lisboa, Instituto Superior Técnico

Santos, A. J. (1995) - Modelo Hidrodinâmico Tridimensional de Circulação Oceânica e Estuarina. Ph. D, Thesis, Universidade Técnica de Lisboa, Instituto Superior Técnico

Taboada J.J., R. Prego, M. Ruiz-Villarreal, P. Montero, M. Gómez-Gesteira, A. Santos and V. Pérez-Villar (1998) - Evaluation of the seasonal variations in the

residual patterns in the Ría de Vigo (NWSpain) by means of a 3D baroclinic model, Estuarine Coastal and Shelf Science 47, pp. 661-670

Taboada, J.J., M. Ruíz-Villarreal, M. Gómez-Gesteira, P. Montero, A. P. Santos, V. Pérez-Villar and R. Prego (2000) - Estudio del transporte en la Ría de Pontevedra (NOEspaña) mediante un modelo 3D: Resultados preliminares, In: Estudos de Biogeoquímica na zona costeira ibérica,Eds. A.Da Costa, C. Vale and R. Prego, Servicio de Publicaciones da Universidade de Aveiro in press.

Villarreal, M.R., P. Montero, R. Prego, J.J. Taboada, P. Leitao, M. Gómez-Gesteira, M. de Castro and V. Pérez-Villar (2000) - Water Circulation in the Ria de Pontevedra under estuarine conditions using a 3d hydrodynamical model, submitted to Est. Coast. and Shelf Sc.

Viollet P.-L. et al., Mécanique des fluides appliquée, Presses de l'école nationale des Ponts et chausses, 1998